Nano Research
2021, 14(7): 2053–2066
ISSN 1998-0124 CN 11-5974/O4
https://doi.org/10.1007/s12274-021-3506-9

Flagship Review

Amorphous carbon-based materials as platform for advanced high-performance anodes in lithium secondary batteries

Jianwei Nai[1,§], Xinyue Zhao[1,§], Huadong Yuan[1,§], Xinyong Tao[1] (✉), and Lin Guo[2] (✉)

[1] College of Materials Science and Engineering, Zhejiang University of Technology, Hangzhou 310014, China
[2] School of Chemistry, Beijing Advanced Innovation Center for Biomedical Engineering, Beihang University, Beijing 100191, China
[§] Jianwei Nai, Xinyue Zhao, and Huadong Yuan contributed equally to this work.

Received: 26 January 2021 / **Revised:** 2 April 2021 / **Accepted:** 7 April 2021

ABSTRACT

The growing concern for the exhaustion of fossil energy and the rapid revolution of electronics have created a rising demand for electrical energy storage devices with high energy density, for example, lithium secondary batteries (LSBs). With high surface area, low cost, excellent mechanical strength, and electrochemical stability, amorphous carbon-based materials (ACMs) have been widely investigated as promising platform for anode materials in the LSBs. In this review, we firstly summarize recent advances in the synthesis of the ACMs with various morphologies, ranging from zero- to three-dimensional structures. Then, the use of ACMs in Li-ion batteries and Li metal batteries is discussed respectively with the focus on the relationship between the structural features of the as-prepared ACMs and their roles in promoting electrochemical performances. Finally, the remaining challenges and the possible prospects for the use of ACMs in the LSBs are proposed to provide some useful clews for the future developments of this attractive area.

KEYWORDS

amorphous, carbon, nanomaterials, lithium secondary batteries, energy storage

1 Introduction

Since the commercialization of rechargeable lithium-ion batteries (LIBs) in the 1990s, LIBs have gradually dominated the market of consumer electronics due to their favorable energy density, long cycle life, negligible memory effect, and environmental friendliness [1, 2]. The growing concern for the exhaustion of fossil energy as well as the rapid evolution of electronics has created a rising demand for electrical energy storage devices with high energy density, such as lithium secondary batteries (LSBs) [1]. One of the most important LSB-based systems developed so far is the rechargeable LIBs, which have obvious advantages of high operating voltage, high energy density, and long cycle life [2–4]. Recently, numerous efforts also turn to more powerful LSBs, for example, the Li-metal batteries (LMBs). In the conventional LIB-based systems, the Li source is provided by the cathodes like $LiFePO_4$ and $LiCoO_2$, while Li-free materials, such as graphite, metal oxides, silicon, tin, etc., are employed as the anodes. In comparison, the LMBs directly use metallic lithium as both the anode and the Li source. The Li-metal anode (LMA) is featured with high theoretical capacity (3,860 $mA{\cdot}h{\cdot}g^{-1}$) and ultralow electrochemical potential (−3.04 V versus standard hydrogen electrode), which sheds new light on constructing high-energy-density LSBs [5, 6]. One such type is the lithium-sulfur (Li-S) batteries that comprise an LMA and a sulfur cathode. Of note, the Li-S batteries can achieve an ultrahigh energy density of 2,567 $Wh{\cdot}kg^{-1}$, which is approximately six times larger than that of LIBs based on graphite anode and $LiCoO_2$ cathode [7, 8]. Undoubtedly, the LIBs and LMBs are two representatively advanced and promising energy storage systems in the field of LSBs.

To achieve high energy density for LSBs, it is crucial to develop high-performance anode materials. In the past decades, carbon-based materials, especially those with micro/nanostructures, have been widely investigated and considered as promising candidates for the anode materials in LSBs due to their acceptable specific capacity, low discharge potential, ultrahigh electrochemical stability, and variably porous structures [9–12]. Recently, amorphous materials have been demonstrated as advanced electrode materials with high-performance for applications in the energy-related fields [13–17]. With regard to the regime of LSBs, although the graphite materials have been commercialized as the anode of LIBs for decades, the low theoretical specific capacity of 372 $mA{\cdot}h{\cdot}g^{-1}$ is gradually unable to satisfy the ever-increasing demand for high-energy-density batteries [18–20]. Therefore, a great number of researchers pay their attention to amorphous carbon-based materials (ACMs), which exhibit higher surface area, lower cost, more abundant sources of precursors (such as corn straw [21], bean dregs [22], wood [23], bamboo [24], peat moss [25], etc.), and more variable nanostructures [9]. More importantly, ACMs can be combined with other high-capacity anode materials such as silicon [25–27], metal oxides, metal sulfides [28–30], and metal phosphides [31], obtaining functional carbon-based composites, which enable the further improvement of specific capacity of LIBs. In addition, the functionalized ACMs are often introduced into the LMA systems to improve their stability, where those ACMs can effectively affect the nucleation and growth behavior of the Li

Address correspondence to Xinyong Tao, tao@zjut.edu.cn; Lin Guo, guolin@buaa.edu.cn

metal, thus addressing the growth of Li dendrites which is the critical issue in this type of batteries [32].

In this review, we mainly focus on summarizing the synthetic methods of the ACMs and their promising applications in the LSBs. Firstly, the synthesis approaches of ACMs are systematically classified and discussed on basis of their nanoscale morphologies, that is, zero-dimensional (0D), one-dimensional (1D), two-dimensional (2D), and three-dimensional (3D) structures. In the following part, we conduct a comprehensive discussion on the potential applications of ACMs, including their specific structural features and general design rules, in constructing advanced anode materials for the LIBs and the LMBs. Finally, the remaining challenges along with the prospects for the future development of ACMs for LSBs are proposed.

2 Synthesis of ACMs

The applications of ACMs in constructing advanced and high-performance anodes are highly dependent on their properties. Therefore, it is very necessary to summarize the relevant synthesis strategies, analyze the formation mechanisms, and investigate the effects of the synthesis methods on the properties of the final ACM-based products. Undoubtedly, this could provide multiple choices and inspirations towards the development of synthetic methods for novel ACMs, thus paving the way for their numerous elegant applications. In this part, the universal and representative synthesis methods for ACMs are introduced from the aspects of their morphologies.

2.1 0D structures

The 0D materials have gained focus among researchers because they exhibit unique properties including the uniform and symmetrical structures, as well as large specific surface areas. Hence, various types of 0D ACMs have been widely applied in the field of batteries, such as carbon quantum dots (CQDs) and carbon nanospheres [32–34]. In this part, we summarize the synthesis methods of 0D nanomaterials of the ACMs applied in the energy storage.

CQDs are a new class of carbon-based nanomaterials with minimal size. The extreme reduction of the particle size towards the quantum system leads to the realization of the maximum properties of quantum effect, available ion diffusion, and high electrochemical activity [35]. Benefiting from the above advantages, CQDs are widely used in energy storage [36]. For instance, Hou et al. reported a large-scale fabrication method of homogeneous CQDs without any auxiliary toxic reagents or surface-active agents [37]. In a typical procedure, CQDs were synthesized from acetone by a one-step NaOH-assisted treatment (Fig. 1(a)). A typical transmission electron microscope (TEM) image shows that these CQDs are monodisperse spherical particles with the diameter of 1.5–3.0 nm (Fig. 1(b)). The templating method has been found to be an important way to obtain 0D ACMs with stable morphology.

Carbon nanosphere is another common kind of 0D ACMs. Attributed to the disordered nature, porosity, and spherical morphology, the amorphous carbon nanospheres allow facile electrolyte/electrode contact and fast Li-ion diffusion, which promotes the anode materials to deliver superior electrochemical performances [38]. Therefore, amorphous carbon nanospheres are regarded as important carbon materials in the field of energy storage. Currently, a number of strategies have been developed to prepare amorphous carbon nanospheres. Tang et al. prepared the hollow carbon nanospheres based on hydrothermal carbonization of glucose in the presence of latex templates [39]. The disordered shell thickness of hollow carbon nanospheres is 12 nm, composed of 2–3 short carbon layers [39]. Etacheri et al. reported the synthesis of 0D amorphous porous carbon spheres (PCSs) via a template-free spray pyrolysis method using sucrose as the carbon source (Fig. 1(c)) [38]. From Figs. 1(d) and 1(e), the obtained PCSs annealed at 1,200 °C (PCS-1200) and 2,300 °C (PCS-2300) show different structure. As the annealing temperature increases, the amorphous structure of PCSs is gradually changed to a local graphite state [38]. In addition to regulate the graphitic degree, heteroatom-doping is another effective strategy to improve the electrochemical performances of carbon spheres, which has been widely

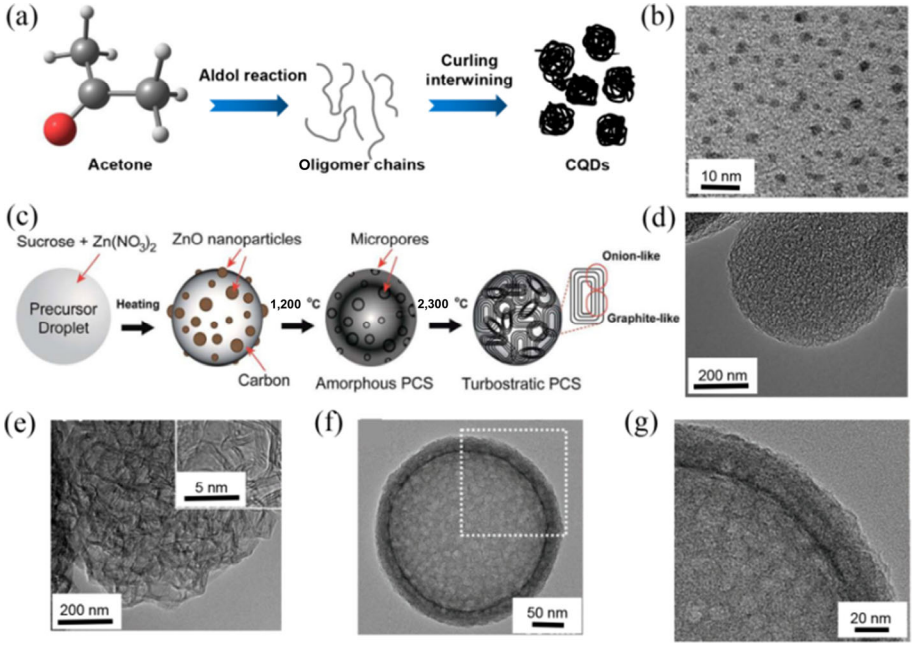

Figure 1 (a) Formation mechanism of CQDs. (b) TEM image of CQDs. Reprinted with permission from Ref. [37], © WILEY-VCH Verlag GmbH & Co. KGaA, Weinheim 2015. (c) Schematic illustration of the synthesis process of the PCSs. (d) High-magnification TEM image of the PCS-1200. (e) High-magnification TEM images of the PCS-2300. Reprinted with permission from Ref. [38], © The Royal Society of Chemistry 2015. (f) TEM image of the N-HPCSs at low magnification. (g) TEM image of the N-HPCSs at high magnification. Reprinted with permission from Ref. [41], © WILEY-VCH Verlag GmbH & Co. KGaA, Weinheim 2020.

applied in the preparation of ACMs to improve the electronic conductivity and enrich active sites for Li-ions storage [39, 40]. Ye et al. reported the synthesis of nitrogen-doped (N-doped) hollow porous carbon spheres (N-HPCSs) [41]. The obtained N-HPCSs with the uniform size exhibit a porous and amorphous structure, and the thickness of the carbon shell as the nitrogen-supporting framework is about 23 nm (Figs. 1(f) and 1(g)). Zhang et al. fabricated a kind of S-doped carbon nanospheres via a hydrothermal synthesis, followed by 800 °C calcination. The S-doped carbon nanospheres with an average size of 500–600 nm maintain ordered channels, which show mesoporous morphology with pore diameters around 3 nm.

2.2 1D structures

1D ACMs show great advantages in energy storage applications due to their unique physical and chemical properties, such as direct ions/electrons paths for their fast transfer and larger specific surface area for facile contact between electrode and electrolyte. Notably, large numbers of synthesis approaches have been developed for 1D ACMs, including templating method [42], electrospinning [43, 44], hydrothermal synthesis [45], magnetron sputtering [46], and so on.

Among a variety of synthesis methods, electrospinning is a simple and effective method to prepare 1D carbon-based nanofibers. By adjusting the parameters of the electrospinning device, nanofibers with unique structures such as coaxial or directional arrangement can be easily obtained [47]. Chen et al. reported amorphous carbon nanotubes decorated with hollow graphitic carbon nanospheres (ACNHGCNs) using a triple-coaxial electrospinning method [48]. The specific synthesis process of ACNHGCNs is illustrated in Figs. 2(a) and 2(b). The walls of the amorphous carbon nanotubes partly consist of hollow graphitic carbon nanospheres, some are decorated on the inside and outside surfaces (Figs. 2(c) and 2(d)) [48]. Further, combining with other methods, such as chemical vapor deposition (CVD), magnetron sputtering and hydrothermal method, electrospinning enables an effective strategy to prepare the structural and compositional features of 1D anode materials. For example, Huang et al. reported a scalable method for the synthesis of flexible half-tube amorphous carbon film by electrospinning and the followed magnetron sputtering, which is composed of carbon nanofibers [46]. The scanning electron microscope (SEM) image indicates the diameter of half-tube amorphous carbon fiber is 20 nm (Fig. 2(e)).

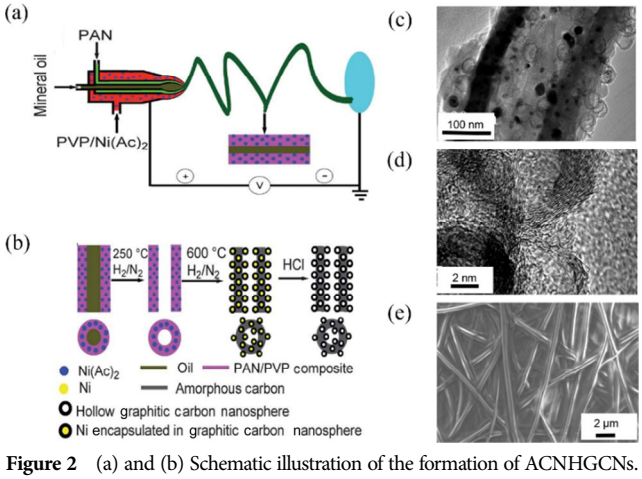

Figure 2 (a) and (b) Schematic illustration of the formation of ACNHGCNs. (c) SEM image of the ACNHGCNs. (d) TEM image of the ACNHGCNs. Reprinted with permission from Ref. [48], © The Royal Society of Chemistry 2012. (e) SEM image of the 20-nm-thick semi-tubular-carbon-coated electrode. Reprinted with permission from Ref. [46], © Elsevier Ltd. 2017.

In addition to electrospinning, the templating method is regarded as a useful method to synthesize 1D amorphous carbon materials. Zhou et al. reported that the Sn nanoparticles were confined within amorphous CNTs (Sn@aCNT) via a nanowire-directed templating method [42]. The diameter of the Sn@aCNT nanorods is about 10 nm [42]. Analogously, by using the MnO_x nanowires as the template and SnO_2 as well as polydopamine as coating materials, a kind of Sn enclosed in N/P-co-doped porous carbon nanorods (Sn@C) was designed by Ye et al. [49]. The length of Sn@C nanorods is 1–2 μm and the diameter is 400–500 nm [49].

2.3 2D structures

As a typical 2D nanomaterials, ACMs have the advantages of large specific surface area, good ionic as well as electronic conductivity, and high mechanical strength [50–52]. Therefore, 2D ACMs have been widely applied in energy storage systems.

Guo et al. synthesized N-doped amorphous carbon nanosheets by thermal decomposition of ethylenediaminetriacetic acid manganese disodium salt (as carbon source) at different temperatures [52]. Figures 3(a) and 3(b) indicate that the as-prepared N-doped carbon nanosheets annealed at 500 °C display an "urchin-like" structure and amorphous characteristic [52]. Compared to single dopant, the synergistic effect of S and N dopants could further realize the improvement of conductivity and interlayer distance for carbon nanosheets. Yang et al. reported a facile sol-gel method for synthesizing amorphous S/N-co-doped carbon nanosheets (S-N/C) using citric acid and urea as the raw materials [53]. Figure 3(c) shows that the interlayer spacing of common carbon nanosheets is 3.4 Å, which increases to 3.47 Å after N doping. As to the carbon nanosheets co-doped with S and N, the lattice spacing further expands to 3.73 Å. As shown in Figs. 3(d) and 3(e), S-N/C show a unique arched tile-like structure [53]. Besides, Wang et al. reported a direct synthesis of amorphous molten-salt carbon nanosheets (MSCs) by adjusting the carbonization temperature of petroleum pitch in molten $KCl/CaCl_2$ (2:1 by weight) (Fig. 3(f)) [54]. Notably, molten salts have been proved to effectively suppress the graphitization of MSCs. The obtained carbon nanosheets display different morphologies at different carbonization temperatures. MSC550, prepared at 550 °C, shows a porous nanostructure with interconnected pores. At the carbonization temperature of 675 °C, the product shows a cheese-like shape with irregular pits on its surface. In addition, when the carbonization is conducted at 800 °C, the product shows a typically folded ultrathin sheet-like structure (Fig. 3(g)) [54].

2.4 3D structures

In the past few decades, more and more researches have been devoted to the synthesis of 3D ACMs. Meanwhile, the properties of 3D ACMs are highly dependent on the template and the preparation methods. Owing to interconnected pores and conductive channels, 3D ACMs demonstrate high potential as anode materials in a variety of batteries.

Due to low cost, environmental friendliness, and abundant resource, renewable biomass materials have been widely used in the fabrication of 3D ACMs for energy storage [55–59]. Shen et al. developed a simple method to produce ultra-thick, low-tortuosity, and mesoporous carbon via directly carbonizing the natural wood (Fig. 4(a)) [23]. Figures 4(b) and 4(c) show the high porosity and low curvature of the obtained carbon materials. There are two different types of pores, with an average size of about 10–15 and 100–200 μm, which originate from plant vessels and cellulose fibers, respectively [23]. Typically, fibrous biomass with cross-linking and porous structures, such

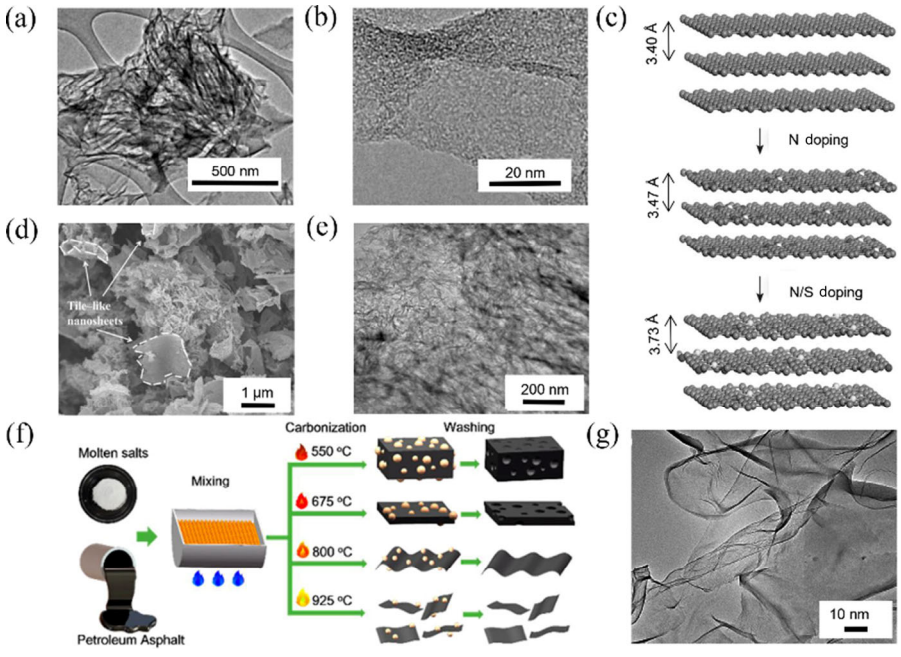

Figure 3 (a) and (b) TEM images of the C-500. Reprinted with permission from Ref. [52], © Elsevier Ltd. 2015. (c) Calculated of layer spacing of graphite, the N/C and the S-N/C. (d) SEM image of the S-N/C. (e) TEM image of the S-N/C. Reprinted with permission from Ref. [53], © WILEY-VCH Verlag GmbH & Co. KGaA, Weinheim 2016. (f) Schematic illustration of the synthetic process of the MSCs. (g) TEM image of the MSC800. Reprinted with permission from Ref. [54], © American Chemical Society 2018.

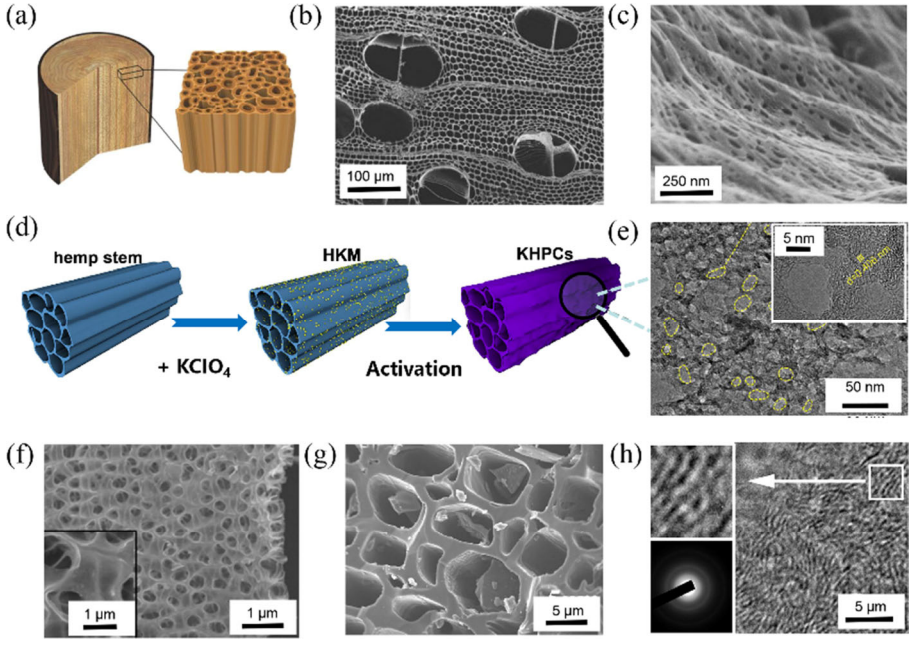

Figure 4 (a) Schematic diagram of natural wood channel. (b) Top-viewed SEM image of wood slabs after carbonization. (c) High-magnification SEM image of (b). Reprinted with permission from Ref. [23], © WILEY-VCH Verlag GmbH & Co. KGaA, Weinheim 2016. (d) Schematic illustration of the synthetic process of the KHPC-600, pre-freeze-dried hemp stem@$KClO_4$ mixture (HKM). (e) TEM images of the KHPC-600. Inset shows the porous structure. Reprinted with permission from Ref. [63], © Elsevier Ltd. 2020. (f) SEM images of hollow macroporous structure of carbon particles. Reprinted with permission from Ref. [25], © American Chemical Society 2013. (g) SEM image of the P-PHC. (h) TEM images and selected-area electron diffraction image of the P-PHC. Reprinted with permission from Ref. [64], © American Chemical Society 2019.

as pistachio shells [58], acori tatarinowii rhizome [60], and pomelo peel [61], are promising precursors for the fabrication of 3D ACMs. Li et al. reported the synthesis of 3D macroporous carbon membrane via carbonization of natural leaves at 1,000 °C [62]. The carbon sheet is 50–100 nm, which facilitates the fast diffusion of the Li ions [62]. Except for carbonized-leaf membrane, Qiu et al. presented a novel method for the synthesis of versatile plant-derived mesopore-dominant hierarchical porous carbon (KHPC) via carbonizing the hemp stem, followed by activation with $KClO_4$ (Fig. 4(d)) [63]. The natural hemp stem displays an open 3D structure composed of micron-scale channels. The pore structures and heteroatom contents within the KHPC can be controlled by adjusting the pyrolysis. After the pyrolysis activation at 600 °C, the KHPC-600 remains the original 3D channel of the hemp stem and shows a hierarchical porous structure that riches in micropores and mesopores (Fig. 4(e)) [63]. Besides, Ding et al. used peat moss, a plant that covers 3% surface of the earth, as a precursor to prepare cross-linked carbon nanosheets [25]. As shown in Fig. 4(f), the product exhibits a hollow 3D structure

with interconnected macropores. The ordered pseudo-graphic structure of nanosheets allows for facile intercalation of Li ions into the bulk carbon [25]. Furthermore, Jiang et al. reported a facile annealing strategy to synthesize pinecone-derived P-doped hive-like carbon (P-PHC) [64]. Figure 4(g) reveals that P-PHC displays a unique 3D structure with obvious large pores, which range from 2–8 μm in diameters. P-PHC manifests segmental graphitization under high-temperature calcination (Fig. 4(h)) [64]. Consequently, on account of abundant source of biomass materials and their various natural pore structures and facile thermal-treatment procedures, biomass-derived 3D ACMs have been anticipated to be promising sustainable materials for energy storage.

The templating method has been found to be an important way to obtain 3D ACMs with stable structure. Liu et al. prepared a kind of SnS_2 ultrathin nanosheets confined in amorphous carbon nanoboxes (SnS_2@CNBs) by templating Fe_2O_3 nanocubes and following an annealing process [65]. The sulfurized particles exhibit the special "nanosheets-in-nanobox" structures. To extend this methodology, the same research group also prepared SnS_2 enclosed hollow carbon nanospheres (SnS_2@CNSs) using SiO_2 spherical template [65]. Wang et al. reported the synthesis of amorphous $CoSnO_3$@C nanoboxes by using $CoSn(OH)_6$ nanoboxes as the hard template [66]. The uniform $CoSnO_3$@C nanoboxes are covered with a carbon shell with a thickness of 30–40 nm [66].

3 Applications of ACMs in LSBs

3.1 Anode materials for LIBs

The materials with suitable discharge potential, high theoretical specific capacity, good electronic conductivity, and excellently structural stability are considered as the ideal anode materials for LIBs [42, 67]. The conventional graphite anode with a low theoretical capacity is unable to meet the needs of advanced LIBs. New types of anode materials with high capacity and high stability need to be explored. Recently, the anode materials such as organic materials, transition metal compounds, metal oxides, silicon, tungsten, tin elements, amorphous carbon and the composite of various materials have been widely applied in LIBs. Among these anode materials, ACMs can be used individually as the anode materials or combined with other materials [68–71]. In the following part, we present some demonstrations of the ACMs applied in the LIBs.

3.1.1 Serving in carbon-based anodes

It is expected that a stable construction of amorphous carbon may ensure a promising electrode with high capacitance and long cycle life. We summarized the electrochemical performance of carbon-based anodes in Table 1 for clear information. Confirmed by previous works, adsorption on the wall of the pores and intercalation between the nanosized graphene layers are two main forms of Li^+ storage in the porous ACMs. However, there are controversies about which one is the dominant. Yang et al. reported the fabrication of 3D porous carbon via pyrolyzing sucrose to investigate the lithium ions storage form in porous ACMs [72]. Nuclear magnetic resonance spectroscopy and cyclic voltammograms are applied to confirm that adsorption is the main form of lithium storage throughout the studied potential range. Nanopores shorten the diffusion distance of lithium ions in electrode materials, so this storage characteristic is the reason for the good electrochemical performance of porous carbon. When the current density is 50 $mA·g^{-1}$, the reversible capacity could reach 400 $mA·h·g^{-1}$ [72].

Amorphous carbons with high specific surface areas, shorter diffusion paths and larger interlayer distances can offer large electrode/electrolyte interfaces for charge-transfer reaction, and enhance ion transport and Li^+ insertion/extraction. Consequently, ACMs are highly recommended for the fabrication of high-performance anodes for LIBs. For instance, Song et al. reported the fabrication of 2D hierarchical amorphous porous carbon nanosheets (HPCS) via a hard templating method [51]. Owing to rich microporous/mesoporous structures and active sites, this kind of material exhibits a high reversible capacity as the anodes for LIBs. When the current density is 20 $mA·g^{-1}$, the reversible capacity could reach 748 $mA·h·g^{-1}$. However, high surface area of HPCS shows more side/edge C atoms and more structural defects, which provide more lithium storage sites. These may be the reasons why initial Coulombic efficiency (CE) of HPCS is only 36% at the current density of 20 $mA·g^{-1}$. As been reported before, low initial CE is an serious

Table 1 Typical carbon-based anodes for LIB applications in reported literatures

Structure	Materials	Initial CE	Reversible capacity	Ref.
0D	Carbon quantum dots	~ 80%	864.9 $mA·h·g^{-1}$ at 0.5 C	[34]
	Porous carbon sphere	70%	365 $mA·h·g^{-1}$ at 37.2 $mA·g^{-1}$	[38]
	Amorphous carbon nanotubes/graphitic carbon nanospheres	~ 60%	969 $mA·h·g^{-1}$ at 50 $mA·g^{-1}$	[48]
1D	Carbon nanofibers	~ 40%	271.7 $mA·h·g^{-1}$ at 30 $mA·g^{-1}$	[119]
	Core–shell structured porous carbon nanowires	86%	811.9 $mA·h·g^{-1}$ at 0.1 $A·g^{-1}$	[120]
2D	Nitrogen-doped carbon nanosheets	39%	465.8 $mA·h·g^{-1}$ at 0.5 C	[52]
	Hierarchical porous nitrogen-doped carbon nanosheets	49.2%	1,865 $mA·h·g^{-1}$ at 0.1 $A·g^{-1}$	[121]
	Hierarchical porous carbon nanosheets	~ 36%	550 $mA·h·g^{-1}$ at 20 $mA·g^{-1}$	[51]
	Porous carbon nanofibers/nanosheets	75%	454 $mA·h·g^{-1}$ at 3 $A·g^{-1}$	[122]
3D	Honey derived mesoporous nitrogen-doped carbons	61%	1,359 $mA·h·g^{-1}$ at 0.1 $A·g^{-1}$	[73]
	Metal-catalyzed graphitic porous carbons	95%	945 $mA·h·g^{-1}$ at 0.2 $A·g^{-1}$	[76]
	Plant-derived mesopore-dominant hierarchical porous carbon	54.7%	1,064 $mA·h·g^{-1}$ at 0.1 $A·g^{-1}$	[63]
	Heteroatom-enriched amorphous carbon with hierarchical porous structure	76%	510–1,090 $mA·h·g^{-1}$ at 50 $mA·g^{-1}$	[69]
	Multilayer graphene film/amorphous porous carbon film	~ 85%	420 $mA·h·g^{-1}$ at 0.1 $A·g^{-1}$	[67]
	Ultrathin amorphous carbon nanosheets	59.4%	731 $mA·h·g^{-1}$ at 0.1 $A·g^{-1}$	[54]
	Sucrose-derived porous carbon	40.1%	400 $mA·h·g^{-1}$ at 50 $mA·g^{-1}$	[72]

phenomenon in amorphous carbon anodes in LIBs, which may result from the decomposition of electrolyte and solid electrolyte interphase (SEI) formation on the high surface [51]. The low initial CE issue could be solved by high-temperature carbonization or chemical reduction to optimize the surface of amorphous carbon and reduce the content of oxygen functional groups. Zhang et al. reported a kind of nitrogen-doped carbons (HMNC) via higher temperature carbonization [73]. The HMNC-700 carbonized at 700 °C for 2 hours shows highly amorphous state (Fig. 5(a)). The HMNC-700 shows an excellent reversible capacity of 1,359 mA·h·g^{-1} at the current density of 100 mA·g^{-1} and superior cycling stability of 722 mA·h·g^{-1} after 200 cycles at the current density of 1 A·g^{-1} (Fig. 5(b)). The excellent electrochemical performance of the HMNC-700 may be attributed to the highly ordered mesopore structures and the corresponding large specific surface areas which can provide large electrode/electrolyte interfaces, more favorable paths for penetration and transportation of ions and serve as Li^+ reservoirs [73]. Additionally, the electrochemical performance of ACMs is significantly improved by doping with heteroatoms in the carbon networks, including N, P, S, and their mixtures [74, 75]. Doping with N has been intensively proven to be an efficient strategy to enhance both the capacity and the cycling stability of amorphous carbon materials. For example, Guo et al. synthesized amorphous nitrogen-doped carbon nanosheets via thermal decomposition, which shows the capacity of 465.8 mA·h·g^{-1} at 0.5 C after 600 cycles.

A kind of 0D amorphous PCSs was fabricated using sucrose as a carbon source via template-free spray pyrolysis method, which have been mentioned above (Fig. 1(e)) [38]. It is obvious that the porosity of the PCSs is retained even after annealing the carbon spheres at 2,300 °C (Fig. 5(c)). The electrode based on amorphous PCS-2300 shows a specific capacity of 270 mA·h·g^{-1} at the current density of 372 mA·g^{-1}, which is four times higher than that of commercial graphite (60 mA·h·g^{-1}) (Fig. 5(d)). After 100 cycles at current densities of 37.2 and 372 mA·g^{-1}, PCS-2300 retains specific capacities of 365 and 250 mA·h·g^{-1}, respectively (Fig. 5(e)). The excellent electrochemical performance of PCSs can be explained by their abundant porosity and disordered structure. Disordered layers of PCS-2300 also facilitate the fast insertion of Li ions to reach excellent specific capacity [38]. Similarly, Yang et al. prepared a kind of metal catalyzed graphite porous carbons (M-GPCs) embedded with amorphous carbon [76]. Different M-GPCs with rich defects and amorphous carbon structures were obtained by adjusting the types of metal catalysts. Figures 5(f) and 5(g) show the nanostructures of Co catalyzed graphite porous carbon (Co-GPC). Graphitic structure defects and the concomitant amorphous carbon can be clearly observed in Co-GPC. Compared with pure graphite materials, Co-GPC exhibits excellent electrochemical performance. At the current density of 3 A·g^{-1}, the electrode based on Co-GPC shows a high capacity of 493 mA·h·g^{-1} after 3,000 cycles (Fig. 5(h)). Such excellent Li-ion storage performance of M-GPCs is mainly due to the amorphous structure with rich active sites and the interconnected graphite structure, which greatly promote the mass transportation and penetration [76]. Therefore, amorphous carbon increases the active sites of lithium ion adsorption in carbon based materials, and improves the overall capacity.

In comparison of pure graphite (372 mA·h·g^{-1}), ACMs with different morphologies exhibit higher specific capacity, which could be ascribed to the following aspects: (1) The redox potential of ACMs (0–1.2 V) is wider than that of the graphite

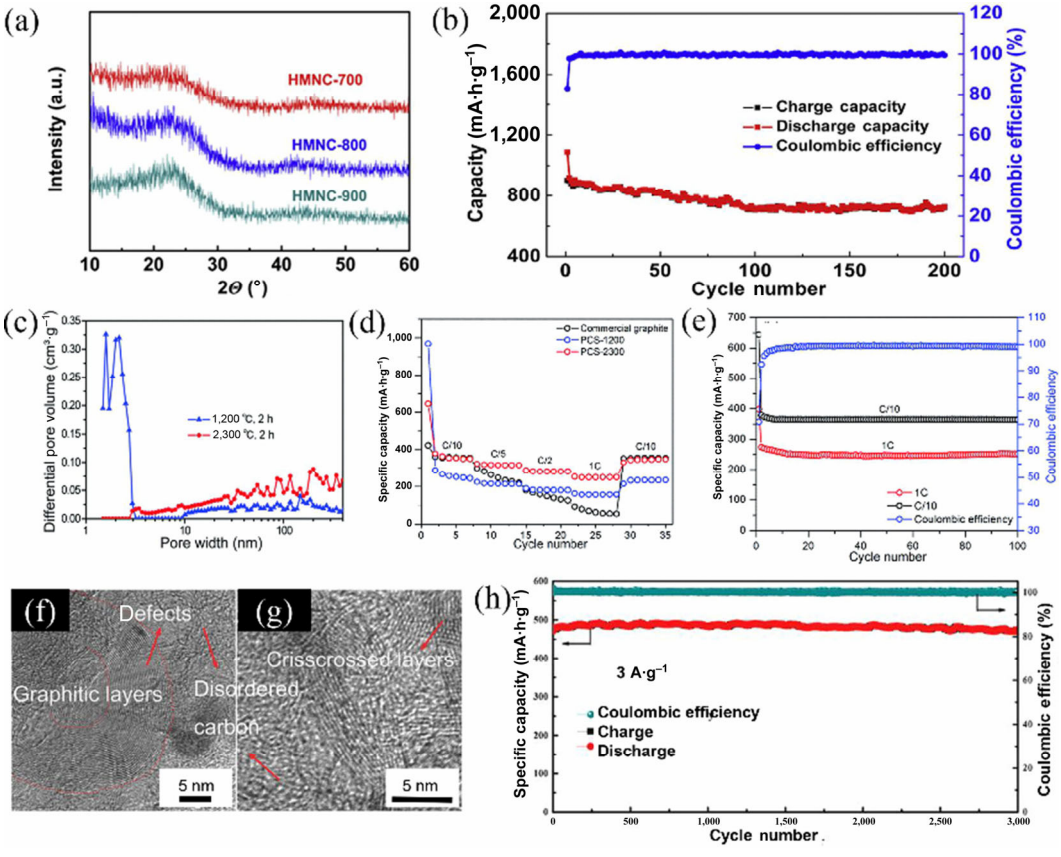

Figure 5 (a) XRD spectra of HMNCs. (b) The cycling performance of HMNC-700 at a current density of 1 A·g^{-1}. Reprinted with permission from Ref. [73], © Elsevier B.V. 2016. (c) Pore size distribution of PCS-1200 and PCS-2300. (d) Electrochemical performances of PCS-1200 and PCS-2300. (e) Galvanostatic cycling performance of PCS-2300 at 0.1 C (0.1 C = 37.2 mA·g^{-1}) and 1 C (1 C = 372 mA·g^{-1}) rate. Reprinted with permission from Ref. [38], © The Royal Society of Chemistry 2015. (f) and (g) TEM images of the Co-GPC. (h) Cycling performance of the Co-GPC at current density of 3 A·g^{-1}. Reprinted with permission from Ref. [76], © WILEY-VCH Verlag GmbH & Co. KGaA, Weinheim 2018.

(0–0.5 V); (2) the expanded interlayer and richer defects in ACMs provide more active sites for the Li-ion storage; (3) the facilely-modified ACMs (that is doped with O, N, S, B, P, etc.) further improve their capacity; (4) the channels in ACMs greatly promote the fast transfer of electrons and lithium ions. Besides, the porous structures in ACMs can also relieve volume change during the process of Li^+ insertion/extraction, enabling the cycling stability of the ACMs. Consequently, ACMs are considered as one of the most attractive anode candidates for the LIBs.

3.1.2 *Serving in non-carbon composite anodes*

Silicon-based materials are considered as one of the attractive anode materials for the next generation LIBs, which is attributed to their high theoretical capacities and low voltage plateau [77]. However, the large volume change of Si-based materials during the cycling processes results in the rapid capacity degradation, limiting their practical applications [78]. In an attempt to suppress the volume change and enhance rate capability, a number of strategies have been developed, such as producing silicon-nanoparticles [78], aligning silicon-nanowires [79]/nanotubes [80], and dispersing silicon into the matrix (e.g. amorphous carbon) [81]. Taking benefit of the high mechanical stability of ACMs, recent reports demonstrate that carbon-silicon composites can suppress the volume change and improve the overall electrochemical performance for LIBs [77, 81]. For example, Fan et al. developed a novel approach to synthesize carbon microspheres/silicon/amorphous carbon by a facile solution-based method using wheat flour as a carbon source and the followed pyrolysis reaction [82]. The amorphous carbon spheres with a size of 20 μm provide a stable conductive carrier for nano-sized silicon, and the overall 3D network structure is beneficial for improving its mechanical stability (Fig. 6(a)). In addition, the amorphous carbon layer with a thickness of 7 nm can also effectively buffer the volume change of silicon particles during the battery cycling, which helps to form a stable SEI between the electrode and the electrolyte (Fig. 6(b)). After 100 cycles, the specific capacity of the electrode based on MSC is 585 $mA{\cdot}h{\cdot}g^{-1}$ at the current density of 100 $mA{\cdot}g^{-1}$, showing a high capacity retention of 90.3% (Fig. 6(c)) [82]. Besides, Yan et al. reported the fabrication of folded carbon nanosheets coated with silicon nanoparticles (Si/C) using one-pot salt melt synthesis [26]. The carbon nanosheets with graphene-like structure are beneficial for the improvement of the conductivity of silicon particles. In addition, the amorphous carbon nanosheets provide limited physical space for the volume expansion of silicon nanoparticles during cycling. After 500 cycles, the Si/C anode can gain 881 $mA{\cdot}h{\cdot}g^{-1}$ at the current density of 420 $mA{\cdot}g^{-1}$ with about 86.4% capacity retained [26]. Silicon material coated with layered N-doped carbon (Si@NPC) is developed through the processes of universal solvent treatment, high pressure sputtering, and carbonization by Liu et al. [27]. The Si@NPC with abundant pores and heteroatom dopants can greatly improve its capability for Li storage. The porous carbon doped with heteroatoms is beneficial for the formation of stable SEI and alleviates the volume expansion of Si during cycling. Therefore, the assembled battery shows a reversible capacity of 1,565 $mA{\cdot}h{\cdot}g^{-1}$ after 100 cycles at 0.5 $A{\cdot}g^{-1}$ [27]. The packaging strategy of ACMs for nanoparticles is also suitable for Sn metal, which has been considered as another promising anode candidate. Zhou et al. reported the fabrication of Sn nanoparticles packaged in amorphous porous carbon nanotubes (Sn@aCNT) using the MnO_x nanowires as the template [42]. The amorphous carbon nanotubes with porous network structure not only inhibit the agglomeration of Sn particles, but also relieve the volume expansion and contraction during the battery cycling (Figs. 6(d) and 6(e)). At the current density of 0.2 $A{\cdot}g^{-1}$, the Sn@aCNT electrode exhibits a high capacity of 749 $mA{\cdot}h{\cdot}g^{-1}$ after 100 cycles (Fig. 6(f)) [42]. Ye et al. developed the synthesis of Sn nanoparticles embedded in N and P co-doped carbon nanorods (N/P-Sn@C) [49]. The Sn nanoparticles are uniformly distributed throughout the carbon nanorods without obvious agglomeration. Due to the homogeneous distribution of Sn nanoparticles in the

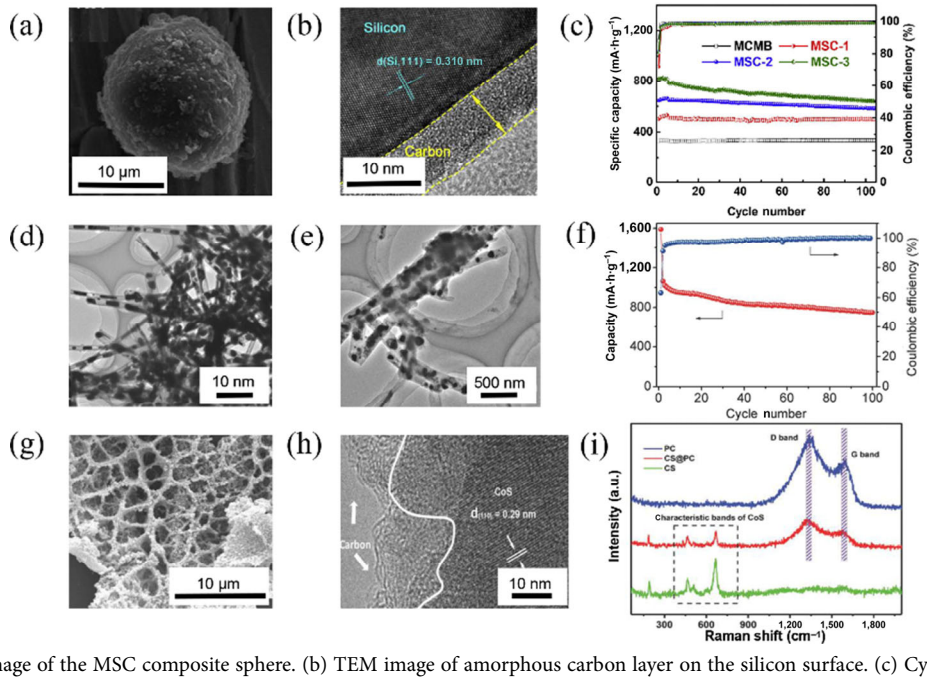

Figure 6 (a) SEM image of the MSC composite sphere. (b) TEM image of amorphous carbon layer on the silicon surface. (c) Cycle performance of the MSC at 100 $mA{\cdot}g^{-1}$. Reprinted with permission from Ref. [82], © Elsevier Ltd. 2019. (d) TEM image of the Sn@aCNT composite. (e) TEM image of the Sn@aCNT electrode after 100 cycles. (f) Cycling performance of the Sn@aCNT electrode at a current density of 0.2 $A{\cdot}g^{-1}$. Reprinted with permission from Ref. [42], © WILEY-VCH Verlag GmbH & Co. KGaA, Weinheim 2016. (g) SEM image of the CS@PC composite. (h) TEM image of the CS@PC composite. (i) Raman scattering spectra of pure carbon (PC), cobalt sulfide without carbon-coated (CS). Reprinted with permission from Ref. [29], © Yin, B. et al. 2018.

amorphous carbon matrix, N/P-Sn@C shows a reversible capacity of 560 mA·h·g^{-1} under the current density of 1 A·g^{-1} after 1,500 cycle [49].

The capacity ranges from 600 to 1,500 mA·h·g^{-1} have made transition metal compounds (TMCs) as another potential anode materials for the LIBs, which is much higher than the theoretical capacity of commercial graphite anode [28, 71]. Nonetheless, TMCs inevitably suffer from several severe challenges, including extensive volume variation during the battery operation, the continuous aggregation of nanoparticles, and poor electronic conductivity, which limit their commercial application [83, 84]. Numerous strategies have been developed to address these problems for Li storage. One useful method is to combine the TMCs with a highly conductive carbon matrix. For example, Yin et al. reported the fabrication of honeycomb-like N/S co-doped porous carbon-coated cobalt sulfide (CS@PC) as an anode material for the LIBs. Figures 6(g) and 6(h) clearly show the honeycomb-like morphology of the CS@PC with the size of tens of microns. Raman spectrum analysis noted that the value of I_D/I_G is 1.22, proving the amorphous structure of the CS@PC (Fig. 6(i)). The CS@PC electrode shows a high capacity of 717 mA·h·g^{-1} at the current density of 1 A·g^{-1} even after 500 cycles. Therefore, the CS@PC electrode exhibits a high specific capacity and stable cycle performance, which could be mainly attributed to the sufficient contact between the electrode and the electrolyte as well as the uniquely amorphous carbon skeleton structure with rich mesoporous [29]. Besides, other TMCs associated with ACMs are also widely applied in the LIBs, such as NiO [85], VO_x [86], Fe_7S_8 [87], ZnO [88], and MoS_2 [89]. To date, there are a great many reports on the ACMs as advanced anode materials for LSBs, which can be attributed to the fact that the ACMs show higher mechanical stability, higher electrical conductivity, and more morphological and porous structures than the graphite.

3.2 Stabilizing Li metal anodes for LMBs

LMA is described as the "Holy Grail" of anode materials used in the LMBs. However, uncontrolled growth of Li metal during the repeated plating/stripping processes, usually embodied as dendritic and mossy Li, induces a series of thorny issues, such as low CE, short circuit, and even fire/explosion of batteries [90, 91]. Recently, researchers have proposed a large number of protective strategies including constructing an artificial SEI [92, 93], designing 3D hosts for Li deposition [94], employing solid-state electrolytes [95–97], and exploiting advanced electrolyte additives [98].

3.2.1 *Serving as artificial SEI*

The SEI between Li metal and electrolyte can act as a protective layer for LMA. However, the naturally formed SEI is not strong enough against the inevitably mechanical deformation of LMA during the repeated cycles due to the limitations of present battery chemistry [99, 100]. In addition, the huge volume variation of Li metal during Li plating/stripping makes the SEI suffer from continuous fracture and regeneration, which further expedites electrolyte decomposition and Li dendrite growth [18]. Constructing additional artificial SEI is considered as an effective method for protecting the LMA [101, 102].

Carbon-based materials are known to be electrochemically stable in battery systems, making an ideal candidate for LMA protection. Some works have explored the potentiality of graphene as artificial SEI for LMA. Nevertheless, due to its conductive feature, part of Li deposits above graphene instead of under it, resulting in poor improvement in CEs (< 95%) [103, 104]. To serve as a stable artificial SEI layer for LMA, the ideal carbon film should be ionically conductive but electronically insulating. Huang et al. reported a scalable method for the synthesis of flexible half-tube amorphous carbon film by electrospinning and the followed magnetron sputtering, which was used as the artificial SEI for the protection of LMA [46]. The SEM measurements are employed to distinguish the morphology difference between the plated Li on bare and 20-nm-thick semi-tubular-carbon-coated Cu electrodes, respectively. Sharp Li dendrites with numerous cracks and pores are clearly formed on the bare Cu (Fig. 7(a)). For comparison, the Li plating on the semi-tubular-carbon coated Cu electrode exhibits a metallic luster without cracked deposits (Fig. 7(b)). It is believed that the amorphous carbon film with low chemical activity and high

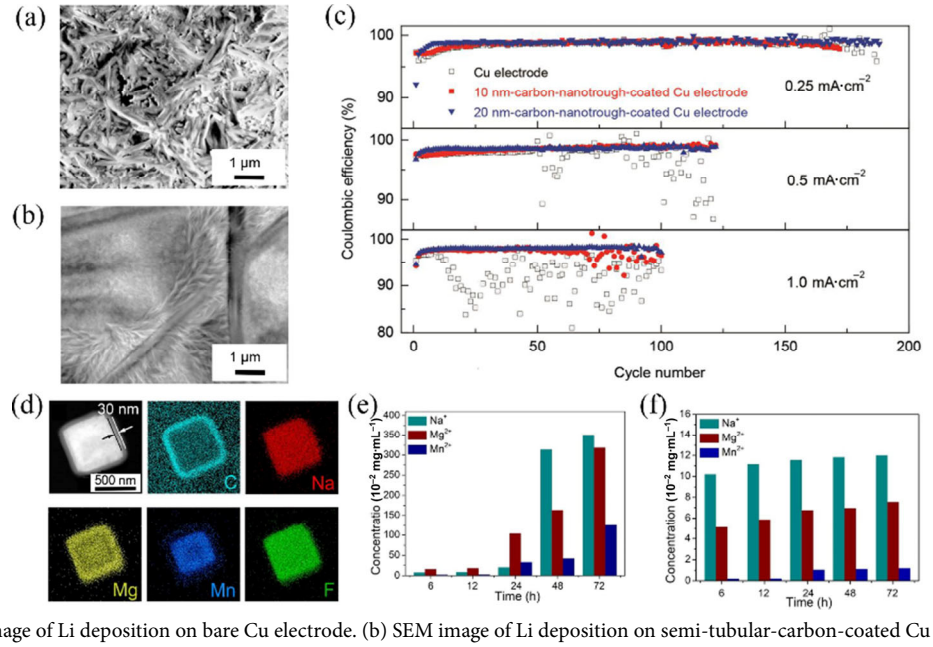

Figure 7 (a) SEM image of Li deposition on bare Cu electrode. (b) SEM image of Li deposition on semi-tubular-carbon-coated Cu electrodes. (c) Cycling performance of Cu|Li asymmetrical cells with bare and semi-tubular-carbon-coated Cu electrodes. Reprinted with permission from Ref. [46], © Elsevier Ltd. 2017. (d) STEM and elemental mapping images of the C, Na, Mg, Mn and F elements. (e) ICP-MS results of the sample from the ether electrolyte containing NMMF. (f) ICP-MS results of the sample from the ether electrolyte containing NMMF@C. Reprinted with permission from Ref. [105], © Yuan, H. D. et al. 2020.

mechanical strength is in favor of the formation of stable SEI. As a result, the ameliorative electrodes display greatly improved cycling stability with high CE up to 99.5% (Fig. 7(c)) [46]. Yuan et al. developed "spansules" that can sustainably supply functional ingredients for the LMA. To be specific, the spansules are made up of NaMg(Mn)F_3@C core@shell microstructures (NMMF@C) via precipitation of fluorides, coating with resin, and high-temperature carbonization [105]. The elemental mapping images of a typical NMMF@C cube exhibit the elemental composition and distribution within the core@shell structures. It is noticed that the amorphous carbon layer is about 30 nm in the periphery region (Fig. 7(d)). Functional ingredients (Na^+, Mg^{2+}, Mn^{2+}, and F^- ions) would be released from the NMMF solid, which could guide the deposit behavior of the Li metal and stabilize the SEI. From the inductively coupled plasma mass spectrometry (ICP-MS) experiments, it is revealed that the dissolution rate of NMMF in the ether electrolyte is reduced with the protection of the amorphous carbon shell (Figs. 7(e) and 7(f)). Further, the mass loss of the NMMF@C is almost linear as a function of time, with the calculated mass loss rate of ~ 0.06 wt.%·h^{-1}. This indicates that the carbon coating of the NMMF@C effectuates stable release of the functional ingredients. The NMMF@C anode exhibits a high CE of 98% after 1,000 cycles at a current density of 2 mA·cm^{-2} [105], which is the most stable LMA reported up to now. In a brief summary, amorphous carbon-based artificial SEI directly coated on Li metal is beneficial for forming stable SEI and decreasing the continuous consumption of active Li and electrolyte, which is of great significance to realize the practical application of LMA in the future.

3.2.2 *Serving as 3D hosts*

ACMs with good electronic conductivity and high specific surface area can not only afford enough channels for electron transfer to reduce the local current density, but also provide enough space for the uniform deposition of Li metal. In addition, ACMs are also beneficial for alleviating the huge volume change during the batteries cycling [106–108]. Therefore, ACMs could be the efficient 3D hosts for Li metal deposition [93, 109–111]. For instance, Liu et al. reported the synthesis of a bendable 3D hollow carbon-based fiber (3D-HCFs) using cotton as precursor for LMA [112]. The Brunauer-Emmett-Teller data indicates that the pore size of hollow carbon fibers is 0.6–2.5 nm (Fig. 8(a)). With the increase of deposition capacity, the morphology of plated Li is still smooth without the appearance of dendritic structure (Fig. 8(b)). The LMA based on 3D-HCFs exhibits a high CE of 99.5% after 300 cycles with a plating capacity of 2 mA·h·cm^{-2} at the current density of 0.5 mA·cm^{-2} (Fig. 8(c)) [112]. Kang et al. reported the synthesis of conductive film via combining amorphous globular carbon grains with polyvinylidene fluoride for stabilizing the LMA [113]. The high special surface area of the amorphous carbon grains significantly reduces the local current density for Li metal deposition. In addition, the pores in amorphous carbon not only provide large space for Li metal deposition, but also inhibit the fracture of SEI films. Due to the high conductivity and high specific surface area of hollow amorphous carbon, numerous kinds of hollow amorphous carbon are widely used in the protection of LMA [32, 94, 106]. For example, Zheng et al. reported a templating method for synthesizing the

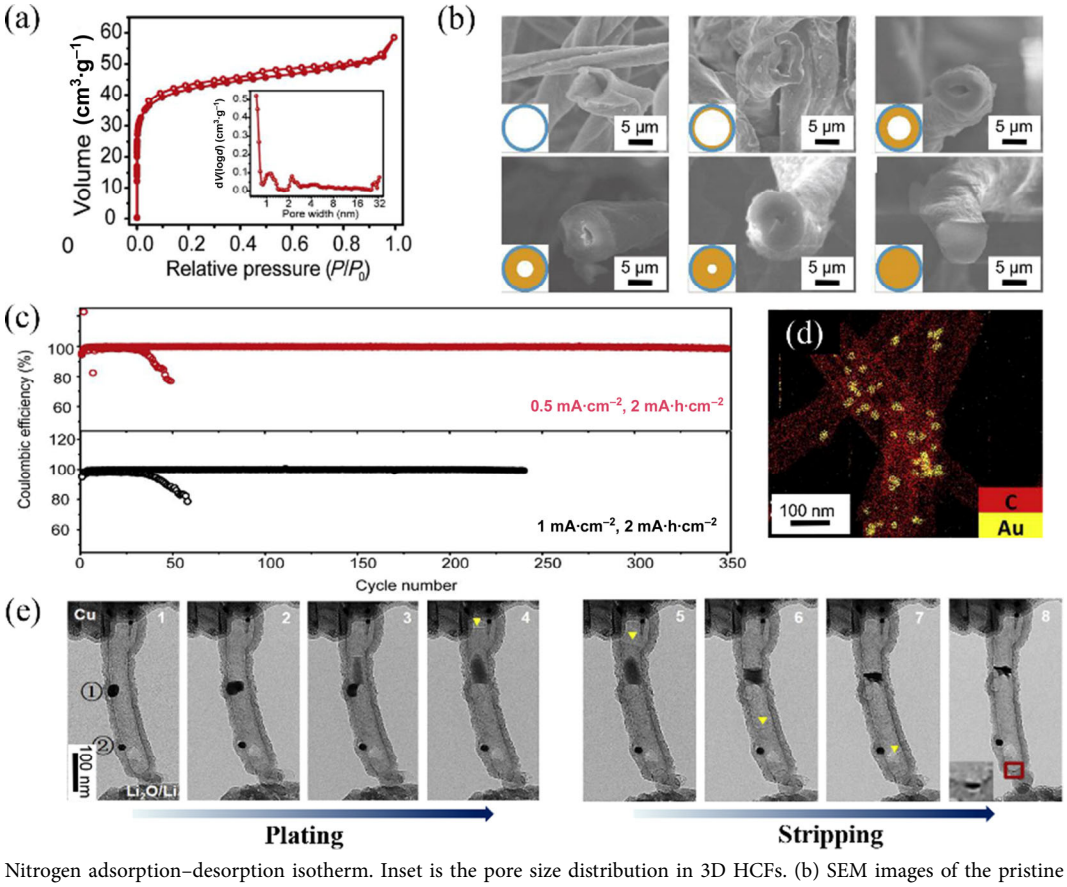

Figure 8 (a) Nitrogen adsorption–desorption isotherm. Inset is the pore size distribution in 3D HCFs. (b) SEM images of the pristine 3D-HCFs and after plating 1, 2, 3, 4, and 6 mA·h·cm^{-2} of Li metal into the 3D-HCFs. (c) Comparison of CE of the 3D-HCFs electrode (solid symbols) and the bare Cu electrode (hollow symbols) with special capacity of 2 mA·h·cm^{-2} at a current density of 0.5 and 1 mA·cm^{-2}. Reprinted with permission from Ref. [112], © Elsevier Inc. 2017. (d) EDS elemental mapping image of the Au@aCNTs. (e) TEM images of Li plating and stripping processes inside an Au@aCNT during the first cycles. Reprinted with permission from Ref. [114], © Elsevier Ltd. 2019.

hollow carbon nanospheres via the deposition of polystyrene [33]. The diameter of hollow carbon nanospheres is 500 nm, and the thickness of carbon wall is around 20 nm. With the increase of plated Li, the uniform nucleation and growth of Li metal on hollow carbon nanospheres without the Li-dendrite structures can be clearly observed, which confirms that Li metal could be uniformly deposited in the constructed carbon spheres [33].

In addition to the construction of favorable structures and morphologies, the modification of lithiophilic groups/additives on amorphous carbon is another effective strategy for suppressing the growth of Li dendrites. Recently, some metals, metal compounds (such as Au [114], Al_2O_3 [32], ZnO [24], etc.) and doping heteroatoms (such as N [41], S [106], etc.) have been applied as efficient seeds to induce the uniform deposition of Li. Lan et al. reported the preparation of Au nanoparticles modified amorphous carbon nanotubes (Au@aCNTs), which act as the plated framework for LMA [114]. Illustrated from the energy-dispersive spectrometer (EDS) elemental mapping of the Au@aCNTs, Au particles with the size of 10 nm are evenly distributed inside the hollow carbon nanotubes (Fig. 8(d)). Figure 8(e) shows the Li deposition and exfoliation processes of Li metal on a single Au@aCNT during the first cycle. At the initial stage of alloying process with Li, the volume of gold particles increases slightly. Subsequently, Li metal nucleates around the gold particles. When Li metal is stripped from the carbon cavity, the Au particles appear in the CNTs again [114]. Analogously, a type of hierarchical porous carbon modified with ZnO quantum dots (ZnO@HPC) was fabricated by Jin et al. [24]. From Fig. 9(a), the average diameter of pores is 0.9 μm, which can be served as the good matrix for Li metal deposition. Meanwhile, the local current density is also believed to be decreased by its porous structure. From Fig. 9(b), a mass of Li dendrites grow on the hierarchical porous carbon (HPC) electrode surface. In contrast, no obvious Li dendrites can be found on the surface of the ZnO@HPC electrode (Fig. 9(c)). The LMA based on 15% ZnO@HPC exhibits a stable cycling life, which can be ascribed that the ZnO nanoparticles are evenly loaded within the HPC and thus induce the growth of Li within the 3D HPC host (Fig. 9(d)). As shown in Fig. 9(e), 15% ZnO@HPC as an anode material for LMBs delivers an average CE of 97.1% at the current density of 1 mA·cm^{-2} after 200 cycles [24].

4 Conclusions and outlook

The past decades have witnessed the development of ACMs for LSBs due to their high surface area, low cost, various structures, and abundant resources. In this review, we have summarized the recent progress of ACMs in LIBs and lithium metal protection, with a specific attention on the aspects of rational synthesis, composition, structure, as well as electrochemical performance.

With the help of fast development of nanotechnology in the field of materials synthesis, a mass of ACMs with various nanostructures from 0D to 3D, mainly including quantum dots, nanospheres, nanofibers, nanosheets, and hierarchical porous structures, have been developed as anode materials for LSBs, gaining substantial achievements. The synthesis methods for ACMs are important as they directly determine the final properties and the possibilities for advanced applications. The commonly used methods for synthesizing 0D ACMs are hydrothermal method and template-free spray pyrolysis. Due to the high surface area, the 0D ACMs are advantageous in the improving of capacity. As for 1D ACMs, the employed methods are template-engaged strategies, electrospinning, and hydrothermal synthesis. The 1D ACMs usually show good mechanical properties and efficient electron diffusion pathways, which is in favor of promoting electronic transport and improving the rate capability. The 2D ACMs can be fabricated by sol-gel methods, thermal decomposition, and molten salt method. Due to the high stability of 2D ACMs during the charge/discharge processes, long-term cycle life can be achieved. Porous 3D ACMs can be obtained from hydrothermal method, templating method, and high-temperature carbonization. ACMs with 3D nanostructures not only create hierarchical porous channels, but also maintain better structural mechanical stability. From a practical point of view, electrode materials with 3D nanostructures exhibit high

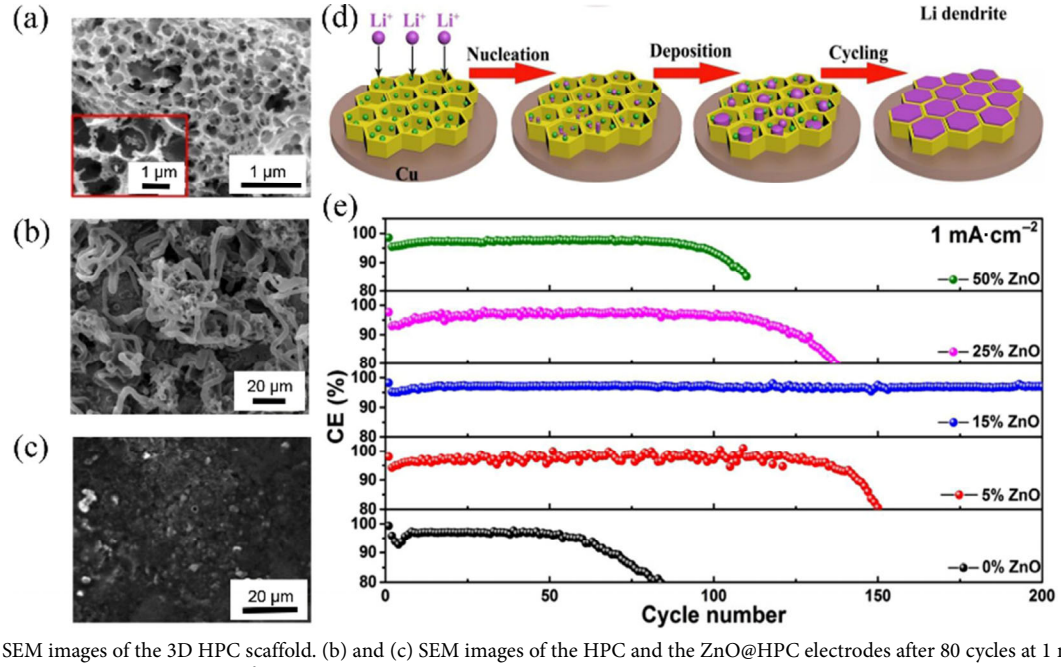

Figure 9 (a) SEM images of the 3D HPC scaffold. (b) and (c) SEM images of the HPC and the ZnO@HPC electrodes after 80 cycles at 1 mA·cm^{-2} with a stripping/plating Li capacity of 1 mA·h·cm^{-2}, respectively. (d) Schematic diagram of Li deposition within the HPC scaffold with the modification of ZnO nanoparticles. (e) The comparison of the CE of Li deposition on pristine HPC and various ZnO@HPC based electrodes at 1 mA·cm^{-2}. Reprinted with permission from Ref. [24], © Elsevier Ltd. 2017.

application prospect for LSBs.

Although the applications of ACMs in LSBs have obtained great progress, there are still several challenges toward the communization in practical battery systems. At the end of this review, we attempt to propose several potential solutions to address the problems:

1) In terms of preparation strategy of ACMs, the precise control of nanostructures is lacked to satisfy the demands of future practical applications for LSBs. Hence, some novel synthesis strategies for ACMs should to be explored and developed. Derenskyi et al. reported the fabrication of carbon nanotubes for the field effect transistors by self-assembly of semiconducting single walled carbon nanotubes (s-SWNTs) on prepatterned substrates [115]. We believe that the self-assembly approaches could inspire the ones for fabricating 1D amorphous carbon with precise nanostructures and might be an attractive research direction. In addition, the self-assembly of lower-dimensional ACMs including CQDs, nanofibers, nanosheets, and hierarchical porous carbon is an effective method to construct ACMs with precise nanostructures, which exhibit unique synergistic effects, revealing the advantage of each unit and overcoming the deficiencies.

2) Due to the high conductivity, high surface area, and abundant channels for ions/electronics transport, the electrodes based on ACMs exhibit high performance for LSBs. However, some preparation processes are not environmentally friendly which prevent the step of ACMs toward practical applications. Therefore, developing simple and green methods for synthesizing ACMs is urgently important, which can meet the ever-increasing demand of LSBs. Biomass in nature with various micro-nano structures has been considered as a kind of promising precursors for ACMs due to the abundant resources, low-cost, and facile treatment procedure. Porous ACMs can be directly obtained by a simple carbonization. This sustainable synthetic method provides the possibility for the commercial development of ACMs.

3) Owing to the irreversible formation of SEI on the surface of the electrodes, the initial CE of electrodes based on ACMs with large surface area is much lower than that of graphite, which seriously hinders the commercial application of ACMs. Improving the initial CE of electrodes based on ACMs becomes an urgent issue to be solved. There are two types of methods to improve initial CE so far: One is reducing the content of oxygen functional groups via high temperature or chemical reduction; the other one is the pre-lithiation, which can achieve the aim of increasing initial CE of ACMs. Nevertheless, developing new methods to improve initial CE is still needed for promoting the performance of ACMs toward practical application.

4) Compared with graphite, the high surface area of ACMs provides abundant pores and large interlayer space for ion storage, resulting in a high capacity. However, the main storage forms of lithium ions in amorphous carbon have not been understood. The internal disorder of the amorphous materials adds the challenge for characterization analysis. With the purpose of understanding the mechanism of ions storage in ACMs, advanced observation techniques should be employed and performed, such as *in-situ* TEM, cryo-transmission electron microscopy (cryo-TEM) [116, 117], nuclear magnetic resonance (NMR), etc. Benefitting from *in-situ* observation techniques, Zhao et al. explored the dominant mechanisms of the phase transformation, structural evolution, and lithiation kinetics of the Bi_2S_3@N-doped mesoporous carbon composite anode [118].

The exciting works summarized in this review are just the tip of the iceberg in the research of ACMs. Despite the undeniable challenges ahead, the development prospect of the ACMs is quite encouraging. With the development of synthetic strategies and analysis methods, ACMs are expected to become unique candidates for constructing advanced anode materials for the commercialization of the LSBs in the future.

Acknowledgments

The authors acknowledge financial support by Leading Innovative and Entrepreneur Team Introduction Program of Zhejiang (No. 2020R01002), the National Natural Science Foundation of China (Nos. 21902144, 51722210, 51972285, and U1802254), and the Natural Science Foundation of Zhejiang Province (Nos. LY17E020010 and LD18E020003).

References

[1] Harper, G.; Sommerville, R.; Kendrick, E.; Driscoll, L.; Slater, P.; Stolkin, R.; Walton, A.; Christensen, P.; Heidrich, O.; Lambert, S. et al. Recycling lithium-ion batteries from electric vehicles. *Nature* **2019**, *575*, 75–86.

[2] Manthiram, A. An outlook on lithium ion battery technology. *ACS Cent. Sci.* **2017**, *3*, 1063–1069.

[3] Cha, H.; Kim, J.; Lee, Y.; Cho, J.; Park, M. Issues and challenges facing flexible lithium-ion batteries for practical application. *Small* **2018**, *14*, 1702989.

[4] Li, M.; Lu, J.; Chen, Z. W.; Amine, K. 30 years of lithium-ion batteries. *Adv. Mater.* **2018**, *30*, 1800561.

[5] Zhang, Y.; Zuo, T. T.; Popovic, J.; Lim, K.; Yin, Y. X.; Maier, J.; Guo, Y. G. Towards better Li metal anodes: Challenges and strategies. *Mater. Today* **2020**, *33*, 56–74.

[6] Shen, K.; Wang, Z.; Bi, X. X.; Ying, Y.; Zhang, D.; Jin, C. B.; Hou, G. Y.; Cao, H. Z.; Wu, L. K.; Zheng, G. Q. et al. Magnetic field-suppressed lithium dendrite growth for stable lithium-metal batteries. *Adv. Energy Mater.* **2019**, *9*, 1900260.

[7] Zhang, A. Y.; Fang, X.; Shen, C. F.; Liu, Y. H.; Seo, I. G.; Ma, Y. Q.; Chen, L.; Cottingham, P.; Zhou, C. W. Functional interlayer of PVDF-HFP and carbon nanofiber for long-life lithium-sulfur batteries. *Nano Res.* **2018**, *11*, 3340–3352.

[8] Liu, T. F.; Hu, H. L.; Ding, X. F.; Yuan, H. D.; Jin, C. B.; Nai, J. W.; Liu, Y. J.; Wang, Y.; Wan, Y. H.; Tao, X. Y. 12 years roadmap of the sulfur cathode for lithium sulfur batteries (2009–2020). *Energy Storage Mater.* **2020**, *30*, 346–366.

[9] Kaskhedikar, N. A.; Maier, J. Lithium storage in carbon nanostructures. *Adv. Mater.* **2009**, *21*, 2664–2680.

[10] Qie, L.; Chen, W. M.; Xiong, X. Q.; Hu, C. C.; Zou, F.; Hu, P.; Huang, Y. H. Sulfur-doped carbon with enlarged interlayer distance as a high-performance anode material for sodium-ion batteries. *Adv. Sci.* **2015**, *2*, 1500195.

[11] Ni, W.; Shi, L. Y. Review article: Layer-structured carbonaceous materials for advanced Li-ion and Na-ion batteries: Beyond graphene. *J. Vac. Sci. Technol. A* **2019**, *37*, 040803.

[12] Balogun, M. S.; Qiu, W. T.; Luo, Y.; Meng, H.; Mai, W. J.; Onasanya, A.; Olaniyi, T. K.; Tong, Y. X. A review of the development of full cell lithium-ion batteries: The impact of nanostructured anode materials. *Nano Res.* **2016**, *9*, 2823–2851.

[13] Cai, Z.; Li, L. D.; Zhang, Y. W.; Yang, Z.; Yang, J.; Guo, Y. J.; Guo, L. Amorphous nanocages of Cu-Ni-Fe Hydr(oxy)oxide prepared by photocorrosion for highly efficient oxygen evolution. *Angew. Chem., Int. Ed.* **2019**, *58*, 4189–4194.

[14] Liu, J. Z.; Hu, Q.; Wang, Y.; Yang, Z.; Fan, X. Y.; Liu, L. M.; Guo, L. Achieving delafossite analog by *in situ* electrochemical self-reconstruction as an oxygen-evolving catalyst. *Proc. Natl. Acad. Sci. USA* **2020**, *117*, 21906–21913.

[15] Liu, J. Z.; Nai, J. W.; You, T. T.; An, P. F.; Zhang, J.; Ma, G. S.; Niu, X. G.; Liang, C. Y.; Yang, S. H.; Guo, L. The flexibility of an amorphous cobalt hydroxide nanomaterial promotes the electrocatalysis of oxygen evolution reaction. *Small* **2018**, *14*, 1703514.

[16] Nai, J. W.; Kang, J. X.; Guo, L. Tailoring the shape of amorphous nanomaterials: Recent developments and applications. *Sci. China Mater.* **2015**, *58*, 44–59.
[17] Nai, J. W.; Yin, H. J.; You, T. T.; Zheng, L. R.; Zhang, J.; Wang, P. X.; Jin, Z.; Tian, Y.; Liu, J. Z.; Tang, Z. Y. et al. Efficient electrocatalytic water oxidation by using amorphous Ni-Co double hydroxides nanocages. *Adv. Energy Mater.* **2015**, *5*, 1401880.
[18] Zhu, J. G.; Li, P. K.; Chen, X.; Legut, D.; Fan, Y. C.; Zhang, R. F.; Lu, Y. Y.; Cheng, X. B.; Zhang, Q. F. Rational design of graphitic-inorganic Bi-layer artificial SEI for stable lithium metal anode. *Energy Storage Mater.* **2019**, *16*, 426–433.
[19] Xiang, H. Q.; Fang, S. B.; Jiang, Y. Y. Mechanism of lithium insertion in carbons pyrolyzed at low temperature. *Chin. Sci. Bull.* **1999**, *44*, 385–390.
[20] Kim, H.; Kim, S. W.; Park, Y. U.; Gwon, H.; Seo, D. H.; Kim, Y.; Kang, K. SnO_2/graphene composite with high lithium storage capability for lithium rechargeable batteries. *Nano Res.* **2010**, *3*, 813–821.
[21] Zhu, Y. E.; Gu, H. C.; Chen, Y. N.; Yang, D. H.; Wei, J. P.; Zhou, Z. Hard carbon derived from corn straw piths as anode materials for sodium ion batteries. *Ionics* **2018**, *24*, 1075–1081.
[22] Yang, T. Z.; Qian, T.; Wang, M. F.; Shen, X. W.; Xu, N.; Sun, Z. Z.; Yan, C. L. A sustainable route from biomass byproduct okara to high content nitrogen-doped carbon sheets for efficient sodium ion batteries. *Adv. Mater.* **2016**, *28*, 539–545.
[23] Shen, F.; Luo, W.; Dai, J. Q.; Yao, Y. G.; Zhu, M. W.; Hitz, E.; Tang, Y. F.; Chen, Y. F.; Sprenkle, V. L.; Li, X. L. et al. Ultra-thick, low-tortuosity, and mesoporous wood carbon anode for high-performance sodium-ion batteries. *Adv. Energy Mater.* **2016**, *6*, 1600377.
[24] Jin, C. B.; Sheng, O. W.; Luo, J. M.; Yuan, H. D.; Fang, C.; Zhang, W. K.; Huang, H.; Gan, Y. P.; Xia, Y.; Liang, C. et al. 3D lithium metal embedded within lithiophilic porous matrix for stable lithium metal batteries. *Nano Energy* **2017**, *37*, 177–186.
[25] Ding, J.; Wang, H. L.; Li, Z.; Kohandehghan, A.; Cui, K.; Xu, Z. W.; Zahiri, B.; Tan, X. H.; Lotfabad, E. M.; Olsen, B. C. et al. Carbon nanosheet frameworks derived from peat moss as high performance sodium ion battery anodes. *ACS Nano* **2013**, *7*, 11004–11015.
[26] Yan, L. J.; Liu, J.; Wang, Q. Q.; Sun, M. H.; Jiang, Z. G.; Liang, C. D.; Pan, F.; Lin, Z. *In situ* wrapping Si nanoparticles with 2D carbon nanosheets as high-areal-capacity anode for lithium-ion batteries. *ACS Appl. Mater. Interfaces* **2017**, *9*, 38159–38164.
[27] Liu, N. T.; Mamat, X.; Jiang, R. Y.; Tong, W.; Huang, Y. D.; Jia, D. Z.; Li, Y. T.; Wang, L.; Wågberg, T.; Hu, G. Z. Facile high-voltage sputtering synthesis of three-dimensional hierarchical porous nitrogen-doped carbon coated Si composite for high performance lithium-ion batteries. *Chem. Eng. J.* **2018**, *343*, 78–85.
[28] Liu, D. H.; Li, W. H.; Zheng, Y. P.; Cui, Z.; Yan, X.; Liu, D. S.; Wang, J. W.; Zhang, Y.; Lü, H. Y.; Bai, F. Y. et al. *In situ* encapsulating α-MnS into N, S-codoped nanotube-like carbon as advanced anode material: α→β phase transition promoted cycling stability and superior Li/Na-storage performance in half/full cells. *Adv. Mater.* **2018**, *30*, 1706317.
[29] Yin, B.; Cao, X. X.; Pan, A. Q.; Luo, Z. G.; Dinesh, S.; Lin, J. D.; Tang, Y.; Liang, S. Q.; Cao, G. Z. Encapsulation of CoS_x nanocrystals into N/S Co-doped honeycomb-like 3D porous carbon for high-performance lithium storage. *Adv. Sci.* **2018**, *5*, 1800829.
[30] Zheng, M. B.; Tang, H.; Hu, Q.; Zheng, S. S.; Li, L. L.; Xu, J.; Pang, H. Tungsten-based materials for lithium-ion batteries. *Adv. Funct. Mater.* **2018**, *28*, 1707500.
[31] Lu, Y.; Wang, T. Y.; Li, X. R.; Zhang, G. X.; Xue, H. G.; Pang, H. Synthetic methods and electrochemical applications for transition metal phosphide nanomaterials. *RSC Adv.* **2016**, *6*, 87188–87212.
[32] Xie, J.; Wang, J. Y.; Lee, H. R.; Yan, K.; Li, Y. Z.; Shi, F. F.; Huang, W.; Pei, A.; Chen, G.; Subbaraman, R. et al. Engineering stable interfaces for three-dimensional lithium metal anodes. *Sci. Adv.* **2018**, *4*, eaat5168.
[33] Zheng, G. Y.; Lee, S. W.; Liang, Z.; Lee, H. W.; Yan, K.; Yao, H. B.; Wang, H. T.; Li, W. Y.; Chu, S.; Cui, Y. Interconnected hollow carbon nanospheres for stable lithium metal anodes. *Nat. Nanotechnol.* **2014**, *9*, 618–623.
[34] Javed, M.; Saqib, A. N. S.; Ata-ur-Rehman; Ali, B.; Faizan, M.; Anang, D. A.; Iqbal, Z.; Abbas, S. M. Carbon quantum dots from glucose oxidation as a highly competent anode material for lithium and sodium-ion batteries. *Electrochim. Acta* **2019**, *297*, 250–257.
[35] Jing, M. J.; Wang, J. F.; Hou, H. S.; Yang, Y. C.; Zhang, Y.; Pan, C. C.; Chen, J.; Zhu, Y. R.; Ji, X. B. Carbon quantum dot coated Mn_3O_4 with enhanced performances for lithium-ion batteries. *J. Mater. Chem. A* **2015**, *3*, 16824–16830.
[36] Hoang, V. C.; Dave, K.; Gomes, V. G. Carbon quantum dot-based composites for energy storage and electrocatalysis: Mechanism, applications and future prospects. *Nano Energy* **2019**, *66*, 104093.
[37] Hou, H. S.; Banks, C. E.; Jing, M. J.; Zhang, Y.; Ji, X. B. Carbon quantum dots and their derivative 3D porous carbon frameworks for sodium-ion batteries with ultralong cycle life. *Adv. Mater.* **2015**, *27*, 7861–7866.
[38] Etacheri, V.; Wang, C. W.; O'Connell, M. J.; Chan, C. K.; Pol, V. G. Porous carbon sphere anodes for enhanced lithium-ion storage. *J. Mater. Chem. A* **2015**, *3*, 9861–9868.
[39] Tang, K.; Fu, L. J.; White, R. J.; Yu, L. H.; Titirici, M. M.; Antonietti, M.; Maier, J. Hollow carbon nanospheres with superior rate capability for sodium-based batteries. *Adv. Energy Mater.* **2012**, *2*, 873–877.
[40] Chen, W. M.; Wan, M.; Liu, Q.; Xiong, X. Q.; Yu, F. Q.; Huang, Y. H. Heteroatom-doped carbon materials: Synthesis, mechanism, and application for sodium-ion batteries. *Small Methods* **2019**, *3*, 1800323.
[41] Ye, W. B.; Pei, F.; Lan, X. N.; Cheng, Y.; Fang, X. L.; Zhang, Q. F.; Zheng, N. F.; Peng, D. L.; Wang, M. S. Stable nano-encapsulation of lithium through seed-free selective deposition for high-performance Li battery anodes. *Adv. Energy Mater.* **2020**, *10*, 1902956.
[42] Zhou, X. S.; Yu, L.; Yu, X. Y.; Lou, X. W. Encapsulating Sn nanoparticles in amorphous carbon nanotubes for enhanced lithium storage properties. *Adv. Energy Mater.* **2016**, *6*, 1601177.
[43] Jiang, W. W.; Liu, Q. H.; Peng, J. F.; Jiang, Y. H.; Ding, Y. H.; Wei, Q. Co_9S_8 nanoparticles embedded into amorphous carbon as anode materials for lithium-ion batteries. *Nanotechnology* **2020**, *31*, 235713.
[44] Xie, W. H.; Li, S. Y.; Wang, S. Y.; Xue, S.; Liu, Z. J.; Jiang, X. Y.; He, D. Y. N-doped amorphous carbon coated Fe_3O_4/SnO_2 coaxial nanofibers as a binder-free self-supported electrode for lithium ion batteries. *ACS Appl. Mater. Interfaces* **2014**, *6*, 20334–20339.
[45] Wang, H.; Tong, Z. Q.; Yang, R.; Huang, Z. M.; Shen, D.; Jiao, T. P.; Cui, X.; Zhang, W. J.; Jiang, Y.; Lee, C. S. Electrochemically stable sodium metal-tellurium/carbon nanorods batteries. *Adv. Energy Mater.* **2019**, *9*, 1903046.
[46] Huang, S. Y.; Tang, L.; Najafabadi, H. S.; Chen, S.; Ren, Z. F. A highly flexible semi-tubular carbon film for stable lithium metal anodes in high-performance batteries. *Nano Energy* **2017**, *38*, 504–509.
[47] Li, X. Y.; Chen, W. C.; Qian, Q. R.; Huang, H. T.; Chen, Y. M.; Wang, Z. Q.; Chen, Q. H.; Yang, J.; Li, J.; Mai, Y. W. Electrospinning-based strategies for battery materials. *Adv. Energy Mater.* **2021**, *11*, 2000845.
[48] Chen, Y. M.; Lu, Z. G.; Zhou, L. M.; Mai, Y. W.; Huang, H. T. Triple-coaxial electrospun amorphous carbon nanotubes with hollow graphitic carbon nanospheres for high-performance Li ion batteries. *Energy Environ. Sci.* **2012**, *5*, 7898–7902.
[49] Ye, X. C.; Lin, Z. H.; Liang, S. J.; Huang, X. H.; Qiu, X. Y.; Qiu, Y. C.; Liu, X. M.; Xie, D.; Deng, H.; Xiong, X. H. et al. Upcycling of electroplating sludge into ultrafine Sn@C nanorods with highly stable lithium storage performance. *Nano Lett.* **2019**, *19*, 1860–1866.
[50] Chen, M.; Zheng, J. H.; Sheng, O. W.; Jin, C. B.; Yuan, H. D.; Liu, T. F.; Liu, Y. J.; Wang, Y.; Nai, J. W.; Tao, X. Y. Sulfur–nitrogen co-doped porous carbon nanosheets to control lithium growth for a stable lithium metal anode. *J. Mater. Chem. A* **2019**, *7*, 18267–18274.
[51] Song, R. R.; Song, H. H.; Zhou, J. S.; Chen, X. H.; Wu, B.; Yang, H. Y. Hierarchical porous carbon nanosheets and their favorable high-rate performance in lithium ion batteries. *J. Mater. Chem.* **2012**, *22*, 12369–12374.
[52] Guo, W.; Li, X.; Xu, J. T.; Liu, H. K.; Ma, J. M.; Dou, S. X. Growth of highly nitrogen-doped amorphous carbon for lithium-ion battery anode. *Electrochim. Acta* **2016**, *188*, 414–420.
[53] Yang, J. Q.; Zhou, X. L.; Wu, D. H.; Zhao, X. D.; Zhou, Z. S-doped N-rich carbon nanosheets with expanded interlayer distance as anode materials for sodium-ion batteries. *Adv. Mater.* **2017**, *29*, 1604108.
[54] Wang, Y. X.; Tian, W.; Wang, L. H.; Zhang, H. R.; Liu, J. L.; Peng, T. Y.; Pan, L.; Wang, X. B.; Wu, M. B. A tunable molten-salt route for

scalable synthesis of ultrathin amorphous carbon nanosheets as high-performance anode materials for lithium-ion batteries. *ACS Appl. Mater. Interfaces* **2018**, *10*, 5577–5585.

[55] Li, Y. M.; Xu, S. Y.; Wu, X. Y.; Yu, J. Z.; Wang, Y. S.; Hu, Y. S.; Li, H.; Chen, L. Q.; Huang, X. J. Amorphous monodispersed hard carbon micro-spherules derived from biomass as a high performance negative electrode material for sodium-ion batteries. *J. Mater. Chem. A* **2015**, *3*, 71–77.

[56] Wang, Z. H.; Shen, D. K.; Wu, C. F.; Gu, S. State-of-the-art on the production and application of carbon nanomaterials from biomass. *Green Chem.* **2018**, *20*, 5031–5057.

[57] Wang, Y. L.; Qu, Q. L.; Gao, S. T.; Tang, G. S.; Liu, K. M.; He, S. J.; Huang, C. B. Biomass derived carbon as binder-free electrode materials for supercapacitors. *Carbon* **2019**, *155*, 706–726.

[58] Xu, S. D.; Zhao, Y.; Liu, S. B.; Ren, X. X.; Chen, L.; Shi, W. J.; Wang, X. M.; Zhang, D. Curly hard carbon derived from pistachio shells as high-performance anode materials for sodium-ion batteries. *J. Mater. Sci.* **2018**, *53*, 12334–12351.

[59] Yuan, H. D.; Liu, T. F.; Liu, Y. J.; Nai, J. W.; Wang, Y.; Zhang, W. K.; Tao, X. Y. A review of biomass materials for advanced lithium-sulfur batteries. *Chem. Sci.* **2019**, *10*, 7484–7495.

[60] Li, Q.; He, T.; Zhang, Y. Q.; Wu, H. Q.; Liu, J. J.; Qi, Y. J.; Lei, Y. P.; Chen, H.; Sun, Z. F.; Peng, C. et al. Biomass waste-derived 3D metal-free porous carbon as a bifunctional electrocatalyst for rechargeable zinc-air batteries. *ACS Sustainable Chem. Eng.* **2019**, *7*, 17039–17046.

[61] Jing, S. Y.; Zhang, Y. L.; Chen, F.; Liang, H. G.; Yin, S. B.; Tsiakaras, P. Novel and highly efficient cathodes for Li-O_2 batteries: 3D self-standing NiFe@NC-functionalized N-doped carbon nanonet derived from Prussian blue analogues/biomass composites. *Appl. Catal. B Environ.* **2019**, *245*, 721–732.

[62] Li, H. B.; Shen, F.; Luo, W.; Dai, J. Q.; Han, X. G.; Chen, Y. N.; Yao, Y. G.; Zhu, H. L.; Fu, K.; Hitz, E. et al. Carbonized-leaf membrane with anisotropic surfaces for sodium-ion battery. *ACS Appl. Mater. Interfaces* **2016**, *8*, 2204–2210.

[63] Qiu, D. P.; Kang, C. H.; Li, M.; Wei, J. Y.; Hou, Z. W.; Wang, F.; Yang, R. Biomass-derived mesopore-dominant hierarchical porous carbon enabling ultra-efficient lithium ion storage. *Carbon* **2020**, *162*, 595–603.

[64] Jiang, Z. L.; Sun, H.; Shi, W. K.; Cheng, J. Y.; Hu, J. Y.; Guo, H. L.; Gao, M. Y.; Zhou, H. J.; Sun, S. G. P-doped hive-like carbon derived from pinecone biomass as efficient catalyst for Li-O_2 battery. *ACS Sustainable Chem. Eng.* **2019**, *7*, 14161–14169.

[65] Liu, Y. H.; Yu, X. Y.; Fang, Y. J.; Zhu, X. S.; Bao, J. C.; Zhou, X. S.; Lou, X. W. Confining SnS_2 ultrathin nanosheets in hollow carbon nanostructures for efficient capacitive sodium storage. *Joule* **2018**, *2*, 725–735.

[66] Wang, Z. Y.; Wang, Z. C.; Liu, W. T.; Xiao, W.; Lou, X. W. Amorphous $CoSnO_3$@C nanoboxes with superior lithium storage capability. *Energy Environ. Sci.* **2013**, *6*, 87–91.

[67] Zhu, D. M.; Liu, H. Q.; Tai, L. X.; Zhang, X. N.; Jiang, S.; Yang, S. M.; Yi, L.; Wen, W.; Li, X. L. Facile construction of novel 3-dimensional graphene/amorphous porous carbon hybrids with enhanced lithium storage properties. *ACS Appl. Mater. Interfaces* **2017**, *9*, 35191–35199.

[68] Hong, W. W.; Ge, P.; Jiang, Y. L.; Yang, L.; Tian, Y.; Zou, G. Q.; Cao, X. Y.; Hou, H. S.; Ji, X. B. Yolk-shell-structured bismuth@N-doped carbon anode for lithium-ion battery with high volumetric capacity. *ACS Appl. Mater. Interfaces* **2019**, *11*, 10829–10840.

[69] Yun, Y. S.; Jin, H. J. Electrochemical performance of heteroatom-enriched amorphous carbon with hierarchical porous structure as anode for lithium-ion batteries. *Mater. Lett.* **2013**, *108*, 311–315.

[70] Li, C. F.; Li, Z. P.; Ye, X. J.; Yang, X. Q.; Zhang, G. Q.; Li, Z. H. Crosslinking-induced spontaneous growth: A novel strategy for synthesizing sandwich-type graphene@Fe_3O_4 dots/amorphous carbon with high lithium storage performance. *Chem. Eng. J.* **2018**, *334*, 1614–1620.

[71] Li, S. Y.; Liu, Y. Y.; Guo, P. S.; Wang, C. X. Self-climbed amorphous carbon nanotubes filled with transition metal oxide nanoparticles for large rate and long lifespan anode materials in lithium ion batteries. *ACS Appl. Mater. Interfaces* **2017**, *9*, 26818–26825.

[72] Yang, G. J.; Li, X. Y.; Guan, Z.; Tong, Y. X.; Xu, B.; Wang, X. F.; Wang, Z. X.; Chen, L. Q. Insights into lithium and sodium storage in porous carbon. *Nano Lett.* **2020**, *20*, 3836–3843.

[73] Zhang, Y. Z.; Chen, L.; Meng, Y.; Xie, J.; Guo, Y.; Xiao, D. Lithium and sodium storage in highly ordered mesoporous nitrogen-doped carbons derived from honey. *J. Power Sources* **2016**, *335*, 20–30.

[74] Jiang, S. X.; Chen, M. F.; Wang, X. Y.; Zhang, Y.; Huang, C.; Zhang, Y. P.; Wang, Y. Honeycomb-like nitrogen and sulfur dual-doped hierarchical porous biomass carbon bifunctional interlayer for advanced lithium-sulfur batteries. *Chem. Eng. J.* **2019**, *355*, 478–486.

[75] Chen, X.; Chen, X. R.; Hou, T. Z.; Li, B. Q.; Cheng, X. B.; Zhang, R.; Zhang, Q. Lithiophilicity chemistry of heteroatom-doped carbon to guide uniform lithium nucleation in lithium metal anodes. *Sci. Adv.* **2019**, *5*, eaau7728.

[76] Yang, W.; Yang, W.; Zhang, F.; Wang, G. X.; Shao, G. J. Hierarchical interconnected expanded graphitic ribbons embedded with amorphous carbon: An advanced carbon nanostructure for superior lithium and sodium storage. *Small* **2018**, *14*, 1802221.

[77] Jeong, S.; Li, X. L.; Zheng, J. M.; Yan, P. F.; Cao, R. G.; Jung, H. J.; Wang, C. M.; Liu, J.; Zhang, J. G. Hard carbon coated nano-Si/graphite composite as a high performance anode for Li-ion batteries. *J. Power Sources* **2016**, *329*, 323–329.

[78] Haro, M.; Singh, V.; Steinhauer, S.; Toulkeridou, E.; Grammatikopoulos, P.; Sowwan, M. Nanoscale heterogeneity of multilayered Si anodes with embedded nanoparticle scaffolds for Li-ion batteries. *Adv. Sci.* **2017**, *4*, 1700180.

[79] Zhang, B. C.; Wang, H.; He, L.; Zheng, C. J.; Jie, J. S.; Lifshitz, Y.; Lee, S. T.; Zhang, X. H. Centimeter-long single-crystalline Si nanowires. *Nano Lett.* **2017**, *17*, 7323–7329.

[80] Liu, R. P.; Shen, C.; Dong, Y.; Qin, J. L.; Wang, Q.; Iocozzia, J.; Zhao, S. Q.; Yuan, K. J.; Han, C. P.; Li, B. H. et al. Sandwich-like CNTs/Si/C nanotubes as high performance anode materials for lithium-ion batteries. *J. Mater. Chem. A* **2018**, *6*, 14797–14804.

[81] Zhang, H.; Zhang, X. F.; Jin, H.; Zong, P.; Bai, Y.; Lian, K.; Xu, H.; Ma, F. A robust hierarchical 3D Si/CNTs composite with void and carbon shell as Li-ion battery anodes. *Chem. Eng. J.* **2019**, *360*, 974–981.

[82] Fan, P.; Mu, T. S.; Lou, S. F.; Cheng, X. Q.; Gao, Y. Z.; Du, C. Y.; Zuo, P. J.; Ma, Y. L.; Yin, G. P. Amorphous carbon-encapsulated Si nanoparticles loading on MCMB with sandwich structure for lithium ion batteries. *Electrochim. Acta* **2019**, *306*, 590–598.

[83] Zheng, M. B.; Tang, H.; Li, L. L.; Hu, Q.; Zhang, L.; Xue, H. G.; Pang, H. Hierarchically nanostructured transition metal oxides for lithium-ion batteries. *Adv. Sci.* **2018**, *5*, 1700592.

[84] Fang, S.; Bresser, D.; Passerini, S. Transition metal oxide anodes for electrochemical energy storage in lithium- and sodium-ion batteries. *Adv. Energy Mater.* **2020**, *10*, 1902485.

[85] Tian, J. Y.; Shao, Q.; Dong, X. J.; Zheng, J. L.; Pan, D.; Zhang, X. Y.; Cao, H. L.; Hao, L. H.; Liu, J. R.; Mai, X. M. et al. Bio-template synthesized NiO/C hollow microspheres with enhanced Li-ion battery electrochemical performance. *Electrochim. Acta* **2018**, *261*, 236–245.

[86] Wu, H. Y.; Qin, M. L.; Wang, W.; Cao, Z.; Liu, Z. Q.; Yu, Q. Y.; Lao, C. Y.; Zhang, D. Y.; Jia, B. R.; He, D. L. et al. Ultrafast synthesis of amorphous VO_x embedded into 3D strutted amorphous carbon frameworks–short-range order in dual-amorphous composites boosts lithium storage. *J. Mater. Chem. A* **2018**, *6*, 7053–7061.

[87] Zhang, Q. B.; Liao, J.; Liao, M.; Dai, J. Y.; Ge, H. L.; Duan, T.; Yao, W. T. One-dimensional Fe_7S_8@C nanorods as anode materials for high-rate and long-life lithium-ion batteries. *Appl. Surf. Sci.* **2019**, *473*, 799–806.

[88] Fernando, J. F. S.; Zhang, C.; Firestein, K. L.; Nerkar, J. Y.; Golberg, D. V. ZnO quantum dots anchored in multilayered and flexible amorphous carbon sheets for high performance and stable lithium ion batteries. *J. Mater. Chem. A* **2019**, *7*, 8460–8471.

[89] Wang, J. G.; Liu, H. Y.; Zhou, R.; Liu, X. R.; Wei, B. Q. Onion-like nanospheres organized by carbon encapsulated few-layer MoS_2 nanosheets with enhanced lithium storage performance. *J. Power Sources* **2019**, *413*, 327–333.

[90] Zhang, B. L.; Shi, H. D.; Ju, Z. J.; Huang, K.; Lian, C.; Wang, Y.; Sheng, O. W.; Zheng, J. H.; Nai, J. W.; Liu, T. F. et al. Arrayed silk fibroin for high-performance Li metal batteries and atomic interface structure revealed by cryo-TEM. *J. Mater. Chem. A* **2020**, *8*, 26045–26054.

[91] Jeong, B. O.; Jeong, S. H.; Park, M. S.; Kim, S.; Jung, Y. Synthesis of amorphous carbon materials for lithium secondary batteries. *J. Nanosci. Nanotechnol.* **2014**, *14*, 7788–7792.
[92] Dong, Q. Y.; Hong, B.; Fan, H. L.; Jiang, H.; Zhang, K.; Lai, Y. Q. Inducing the formation of *in situ* Li_3N-rich SEI via nanocomposite plating of Mg_3N_2 with lithium enables high-performance 3D lithium-metal batteries. *ACS Appl. Mater. Interfaces* **2020**, *12*, 627–636.
[93] Ju, Z. J.; Jin, C. B.; Yuan, H. D.; Yang, T.; Sheng, O. W.; Liu, T. F.; Liu, Y. J.; Wang, Y.; Ma, F. Y.; Zhang, W. K.; Nai, J. W. et al. A fast-ion conducting interface enabled by aluminum silicate fibers for stable Li metal batteries. *Chem. Eng. J.* **2021**, *408*, 128016.
[94] Liu, S. F.; Xia, X. H.; Zhong, Y.; Deng, S. J.; Yao, Z. J.; Zhang, L. Y.; Cheng, X. B.; Wang, X. L.; Zhang, Q.; Tu, J. P. 3D TiC/C core/shell nanowire skeleton for dendrite-free and long-life lithium metal anode. *Adv. Energy Mater.* **2018**, *8*, 1702322.
[95] Wang, C. H.; Bai, G. L.; Yang, Y. F.; Liu, X. J.; Shao, H. X. Dendrite-free all-solid-state lithium batteries with lithium phosphorous oxynitride-modified lithium metal anode and composite solid electrolytes. *Nano Res.* **2019**, *12*, 217–223.
[96] Wang, Z. J.; Yang, K.; Song, Y. L.; Lin, H.; Li, K.; Cui, Y. H.; Yang, L. Y.; Pan, F. Polymer matrix mediated solvation of $LiNO_3$ in carbonate electrolytes for quasi-solid high-voltage lithium metal batteries. *Nano Res.* **2020**, *13*, 2431–2437.
[97] Liu, T. F.; Zheng, J. L.; Hu, H. L.; Sheng, O. W.; Ju, Z. J.; Lu, G. X.; Liu, Y. J.; Nai, J. W.; Wang, Y.; Zhang, W. K. et al. *In-situ* construction of a Mg-modified interface to guide uniform lithium deposition for stable all-solid-state batteries. *J. Energy Chem.* **2021**, *55*, 272–278.
[98] Chen, S. R.; Zheng, J. M.; Yu, L.; Ren, X. D.; Engelhard, M. H.; Niu, C. J.; Lee, H.; Xu, W.; Xiao, J.; Liu, J. et al. High-efficiency lithium metal batteries with fire-retardant electrolytes. *Joule* **2018**, *2*, 1548–1558.
[99] Han, B.; Feng, D. Y.; Li, S.; Zhang, Z.; Zou, Y. C.; Gu, M.; Meng, H.; Wang, C. Y.; Xu, K.; Zhao, Y. S. et al. Self-regulated phenomenon of inorganic artificial solid electrolyte interphase for lithium metal batteries. *Nano Lett.* **2020**, *20*, 4029–4037.
[100] Wang, R.; Yu, J.; Tang, J. T.; Meng, R. J.; Nazar, L. F.; Huang, L. Z.; Liang, X. Insights into dendrite suppression by alloys and the fabrication of a flexible alloy-polymer protected lithium metal anode. *Energy Storage Mater.* **2020**, *32*, 178–184.
[101] Ma, L.; Kim, M. S.; Archer, L. A. Stable artificial solid electrolyte interphases for lithium batteries. *Chem. Mater.* **2017**, *29*, 4181–4189.
[102] Zhong, Y. C.; Chen, Y. M.; Cheng, Y. F.; Fan, Q. L.; Zhao, H. J.; Shao, H. Y.; Lai, Y. Q.; Shi, Z. C.; Ke, X.; Guo, Z. P. Li alginate-based artificial SEI layer for stable lithium metal anodes. *ACS Appl. Mater. Interfaces* **2019**, *11*, 37726–37731.
[103] Yan, K.; Lee, H. W.; Gao, T.; Zheng, G. Y.; Yao, H. B.; Wang, H. T.; Lu, Z. D.; Zhou, Y.; Liang, Z.; Liu, Z. F. et al. Ultrathin two-dimensional atomic crystals as stable interfacial layer for improvement of lithium metal anode. *Nano Lett.* **2014**, *14*, 6016–6022.
[104] Kim, J. S.; Kim, D. W.; Jung, H. T.; Choi, J. W. Controlled lithium dendrite growth by a synergistic effect of multilayered graphene coating and an electrolyte additive. *Chem. Mater.* **2015**, *27*, 2780–2787.
[105] Yuan, H. D.; Nai, J. W.; Tian, H.; Ju, Z. J.; Zhang, W. K.; Liu, Y. J.; Tao, X. Y.; Lou, X. W. An ultrastable lithium metal anode enabled by designed metal fluoride spansules. *Sci. Adv.* **2020**, *6*, eaaz3112.
[106] Zhang, F.; Liu, X. Y.; Yang, M. H.; Cao, X. Q.; Huang, X. Y.; Tian, Y.; Zhang, F.; Li, H. X. Novel S-doped ordered mesoporous carbon nanospheres toward advanced lithium metal anodes. *Nano Energy* **2020**, *69*, 104443.
[107] Kang, C.; Lahiri, I.; Baskaran, R.; Kim, W. G.; Sun, Y. K.; Choi, W. 3-Dimensional carbon nanotube for Li-ion battery anode. *J. Power Sources* **2012**, *219*, 364–370.
[108] Wang, Q.; Yang, C. K.; Yang, J. J.; Wu, K.; Qi, L. Y.; Tang, H.; Zhang, Z. Y.; Liu, W.; Zhou, H. H. Stable Li metal anode with protected interface for high-performance Li metal batteries. *Energy Storage Mater.* **2018**, *15*, 249–256.
[109] An, Y. L.; Tian, Y.; Li, Y.; Wei, C. L.; Tao, Y.; Liu, Y. P.; Xi, B. J.; Xiong, S. L.; Feng, J. K.; Qian, Y. T. Heteroatom-doped 3D porous carbon architectures for highly stable aqueous zinc metal batteries and non-aqueous lithium metal batteries. *Chem. Eng. J.* **2020**, *400*, 125843.
[110] Wang, Z. Y.; Lu, Z. X.; Guo, W.; Luo, Q.; Yin, Y. H.; Liu, X. B.; Li, Y. S.; Xia, B. Y.; Wu, Z. P. A dendrite-free lithium/carbon nanotube hybrid for lithium-metal batteries. *Adv. Mater.* **2021**, *33*, 2006702.
[111] Zhang, R.; Chen, X.; Shen, X.; Zhang, X. Q.; Chen, X. R.; Cheng, X. B.; Yan, C.; Zhao, C. Z.; Zhang, Q. Coralloid carbon fiber-based composite lithium anode for robust lithium metal batteries. *Joule* **2018**, *2*, 764–777.
[112] Liu, L.; Yin, Y. X.; Li, J. Y.; Li, N. W.; Zeng, X. X.; Ye, H.; Guo, Y. C.; Wan, L. J. Free-standing hollow carbon fibers as high-capacity containers for stable lithium metal anodes. *Joule* **2017**, *1*, 563–575.
[113] Kang, H. K.; Woo, S. G.; Kim, J. H.; Lee, S. R.; Kim, Y. J. Conductive porous carbon film as a lithium metal storage medium. *Electrochim. Acta* **2015**, *176*, 172–178.
[114] Lan, X. N.; Ye, W. B.; Zheng, H. F.; Cheng, Y.; Zhang, Q. B.; Peng, D. L.; Wang, M. S. Encapsulating lithium and sodium inside amorphous carbon nanotubes through gold-seeded growth. *Nano Energy* **2019**, *66*, 104178.
[115] Derenskyi, V.; Gomulya, W.; Talsma, W.; Salazar-Rios, J. M.; Fritsch, M.; Nirmalraj, P.; Riel, H.; Allard, S.; Scherf, U.; Loi, M. A. On-chip chemical self-assembly of semiconducting single-walled carbon nanotubes (SWNTs): Toward robust and scale invariant SWNTs transistors. *Adv. Mater.* **2017**, *29*, 1606757.
[116] Sheng, O. W.; Zheng, J. H.; Ju, Z. J.; Jin, C. B.; Wang, Y.; Chen, M.; Nai, J. W.; Liu, T. F.; Zhang, W. K.; Liu, Y. J. et al. *In situ* construction of a LiF-enriched interface for stable all-solid-state batteries and its origin revealed by cryo-TEM. *Adv. Mater.* **2020**, *32*, 2000223.
[117] Li, Y. Z.; Li, Y. B.; Pei, A.; Yan, K.; Sun, Y. M.; Wu, C. L.; Joubert, L. M.; Chin, R.; Koh, A. L.; Yu, Y. et al. Atomic structure of sensitive battery materials and interfaces revealed by cryo–electron microscopy. *Science* **2017**, *358*, 506–510.
[118] Zhao, L. Z.; Wu, H. H.; Yang, C. H.; Zhang, Q. B.; Zhong, G. M.; Zheng, Z. M.; Chen, H. X.; Wang, J. M.; He, K.; Wang, B. L. et al. Mechanistic origin of the high performance of yolk@shell Bi_2S_3@N-doped carbon nanowire electrodes. *ACS Nano* **2018**, *12*, 12597–12611.
[119] Tao, L.; Huang, Y. B.; Yang, X. Q.; Zheng, Y. W.; Liu, C.; Di, M. W.; Zheng, Z. F. Flexible anode materials for lithium-ion batteries derived from waste biomass-based carbon nanofibers: I. Effect of carbonization temperature. *RSC Adv.* **2018**, *8*, 7102–7109.
[120] Chen, F.; Yu, C. P.; Cui, J. W.; Yu, D. B.; Song, P.; Wang, Y.; Qin, Y. Q.; Yan, J.; Wu, Y. C. A core-shell structured metal-organic frameworks-derived porous carbon nanowires as a superior anode for alkaline metal-ion batteries. *Appl. Surf. Sci.* **2021**, *541*, 148473.
[121] Hou, J. H.; Cao, C. B.; Idrees, F.; Ma, X. L. Hierarchical porous nitrogen-doped carbon nanosheets derived from silk for ultrahigh-capacity battery anodes and supercapacitors. *ACS Nano* **2015**, *9*, 2556–2564.
[122] Wang, S. B.; Xiao, C. L.; Xing, Y. L.; Xu, H. Z.; Zhang, S. C. Carbon nanofibers/nanosheets hybrid derived from cornstalks as a sustainable anode for Li-ion batteries. *J. Mater. Chem. A* **2015**, *3*, 6742–6746.